Heterozygosity at a conserved candidate sex determination locus is associated with female development in the clonal raider ant

Kip D. Lacy[1*], Jina Lee[1], Kathryn Rozen-Gagnon[2,3], Wei Wang[3], Thomas S. Carroll[3], Daniel J.C. Kronauer[1,4*]

[1]Laboratory of Social Evolution and Behavior, The Rockefeller University, New York, NY, USA.

[2]Department of Molecular Genetics, University of Toronto, Toronto, Canada.

[3]Bioinformatics Resource Center, The Rockefeller University, New York, NY, USA.

[4]Howard Hughes Medical Institute, New York, NY, USA.

[*]Email: klacy@rockefeller.edu (K.D.L.); dkronauer@rockefeller.edu (D.J.C.K)

Abstract

Sex determination is a developmental switch that triggers sex-specific developmental programs. This switch is "flipped" by the expression of genes that promote male- or female-specific development. Many lineages have evolved sex chromosomes that act as primary signals for sex determination. However, haplodiploidy (males are haploid and females are diploid), which occurs in ca. 12% of animal species, is incompatible with sex chromosomes. Haplodiploid taxa must, therefore, rely on other strategies for sex determination. One mechanism, "complementary sex determination" (CSD), uses heterozygosity as a proxy for diploidy. In CSD, heterozygosity at a sex determination locus triggers female development, while hemizygosity or homozygosity permits male development. CSD loci have been mapped in honeybees and two ant species, but we know little about their evolutionary history. Here, we investigate sex determination in the clonal raider ant, *Ooceraea biroi*. We identified a 46kb candidate CSD locus at which all females are heterozygous, but diploid males are homozygous for either allele. As expected for CSD loci, the candidate locus has more alleles than most other loci, resulting in a peak of nucleotide diversity. This peak negligibly affects the amino acid sequences of protein-coding genes, suggesting that heterozygosity of a non-coding genomic sequence triggers female development. This locus is distinct from the CSD locus in honeybees but homologous to a CSD locus mapped in two distantly related ant species, implying that this molecular mechanism has been conserved since a common ancestor that lived approximately 112 million years ago.

Introduction

Whether an animal develops as a male or a female is typically determined by a switch early in development. This switch, known as sex determination, is a multistep process beginning with primary sex determination signals triggering sex-specific splicing of downstream transcription factors that encode sexual identity (Williams and Carroll 2009). Although the downstream transcription factors are evolutionarily conserved, primary sex determination signals are evolutionarily labile and comprise a diverse range of environmental and genetic mechanisms (Bachtrog et al. 2014). Genetically encoded primary signals (sex-determining genes or chromosomes) are usually found in only one sex. Such systems do not work in haplodiploid taxa (an estimated 12% of animal species, including ants (Normark 2003)), where any allele on any homologous chromosome can be transmitted from diploid females to their haploid male sons, and all alleles experience selection to be viably transmitted from both sexes (Whiting 1935). Haplodiploids, therefore, require alternative sex determination mechanisms, but we know little about the molecular details.

Some parasitoid wasps use a mechanism involving maternal imprinting (Verhulst et al. 2010; Zou et al. 2020). However, in many Hymenoptera, inbred crosses produce diploid males, which led to the hypothesis that female development is triggered by heterozygosity as a proxy for diploidy (Whiting 1933; Whiting 1943). Under this “complementary sex determination” (CSD) hypothesis, different alleles at a given sex determination locus “complement” one another, meaning that heterozygosity triggers female development (**Fig. 1A**). By contrast, the presence of a single allele (either because the individual is haploid or because a diploid individual is homozygous at the sex determination locus) permits male development. Under CSD, diploid males produce diploid sperm and, therefore, are functionally sterile (van

Wilgenburg et al. 2006). This imposes selection for homozygosity avoidance, often meaning obligatory outbreeding. At the gene level, there is negative frequency-dependent (balancing) selection on CSD loci, resulting in the co-occurrence of many alleles at similar frequencies within populations.

Having been a favored hypothesis for more than half a century, CSD was demonstrated in the honeybee *Apis mellifera* in 2003 (Beye et al. 2003). In *A. mellifera*, biallelic heteromers of the protein encoded by the *complementary sex determiner* (*csd*) gene trigger female development, whereas monoallelic homomers permit male development (Beye et al. 2003; Beye et al. 2013; Otte et al. 2023; Seiler and Beye 2024). Although this primary sex determination signal differs from primary signals in other insects, it nonetheless converges upon the pathway that transduces sex determination signals in most insects (Bopp et al. 2014; Wexler et al. 2019). The Csd protein sex-specifically splices the closely linked splicing factor *feminizer* (*fem*) (the honeybee version of *transformer* (*tra*) in *Drosophila* and other insects), which in turn leads to the production of sex-specific isoforms of *doublesex* (*dsx*), a transcription factor that regulates sex-specific development (Hasselmann et al. 2008; Gempe et al. 2009; Verhulst et al. 2010; Zou et al. 2020). Intriguingly, *csd* is a paralog of *fem*. Following the prediction that CSD loci should evolve under balancing selection, many *csd* alleles are held at similar frequencies, and the locus bears signatures of adaptive evolution (Hasselmann and Beye 2004), with amino acid-level heterozygosity in certain protein domains required for female development (Otte et al. 2023).

CSD is assumed to occur in many Hymenoptera that occasionally produce diploid males (van Wilgenburg et al. 2006). Until recently, however, heterozygosity-dependent female development had not been demonstrated outside of *A. mellifera*, which remained the only species for which a CSD locus had been genetically mapped. A recent genetic mapping study in the

wasp *Lysiphlebus fabarum* identified at least one and as many as four candidate sex determination loci (Matthey-Doret et al. 2019) (the multi-locus extension of the CSD hypothesis proposes that heterozygosity at any of multiple sex determination loci is sufficient to trigger female development (Crozier 1971) (**Fig. 1B**)). However, a requirement of heterozygosity at these loci for female development was not demonstrated. In the ant *Vollenhovia emeryi*, a mapping study found two sex determination QTL (Miyakawa and Mikheyev 2015), with follow-up work suggesting that these function as a multi-locus CSD system (Miyakawa and Miyakawa 2023). One of these QTL (*V.emeryiCsdQTL1*) contains two closely linked *tra* homologs, reminiscent of the locus containing *csd* and *fem* in *A. mellifera*. By contrast, the other QTL (*V.emeryiCsdQTL2*) only contains genes without annotated functions in sexual development. Although *V. emeryi* sex determination is likely integrated through *tra* and *dsx*, the molecular basis of their primary sex determination signals remains unclear (Miyakawa et al. 2018; Miyakawa and Miyakawa 2023).

Recently, a sex determination locus was identified in the Argentine ant, *Linepithema humile* (Pan et al. 2024). Consistent with CSD, all pairwise heterozygous combinations of the seven identified alleles were found in females, whereas diploid males were invariably homozygous for one of the seven alleles. Moreover, these alleles occurred at roughly equal frequencies within populations, suggesting evolution under balancing selection. The mapped locus is located within a noncoding genomic region tightly linked to *ant noncoding transformer splicing regulator* (*ANTSR*), a long noncoding RNA (lncRNA) with previously uncharacterized function. *ANTSR* knockdown in female-destined embryos leads to male-specific splicing of *tra*, suggesting that this lncRNA transduces the primary sex determination signal encoded by the heterozygosity (or hemi- or homozygosity) of the linked noncoding region (Pan et al. 2024).

Because the synteny of this region (including the presence of a lncRNA putatively homologous to *ANTSR*) is conserved across the ants, bees, and vespoid wasps, it was suggested that this molecular mechanism may be deeply conserved among the Aculeata (Pan et al. 2024). However, genetic mapping of sex determination has yet to be performed in most of these taxa.

To explore the evolution of sex determination across ants, we investigated the topic in the clonal raider ant, *Ooceraea biroi*. Diploid males occur sporadically in this species, suggesting that, like other ants, it might employ CSD (Kronauer et al. 2012). *O. biroi* reproduces via a mode of parthenogenesis in which two haploid nuclei from a single meiosis fuse to produce diploid offspring (central fusion automixis) (Oxley et al. 2014). Although heterozygosity is maintained with high fidelity despite meiotic crossover recombination (Lacy et al. 2024), losses of heterozygosity occur occasionally, probably due to the inheritance of one recombined and one non-recombined version of a homologous chromosome (Kronauer et al. 2012; Oxley et al. 2014; Trible et al. 2023; Lacy et al. 2024). Therefore, if *O. biroi* uses CSD, diploid males might result from losses of heterozygosity at sex determination loci (**Fig. 1C**). Here, we use whole genome sequencing to map a sex determination locus, demonstrate that most diploid males carry a loss of heterozygosity at this locus, assess the homology of this locus with other sex determination loci, and explore whether balancing selection has shaped evolution at this locus.

Results

Identification of a candidate sex determination locus on chromosome 4

To map sex determination loci in *O. biroi*, we first identified males based on sexual dimorphism and distinguished diploid from haploid males based on heterozygosity at seven genetic markers (**supplementary table S1, file S1, and fig. S1**). We then sequenced the

genomes of 16 diploid males and compared them with 19 previously sequenced genomes of diploid females (Trible et al. 2023; Lacy et al. 2024) (descriptions and metadata for all genomes sequenced in this study are in **supplementary table S2**). CSD loci must be heterozygous to trigger female development but can be homozygous in diploid males. To identify such sites, we calculated a "CSD index" for each single nucleotide polymorphism (SNP), which equals zero if any female is homozygous and equals the proportion of diploid males that are homozygous if all females are heterozygous. We found a peak of the CSD index on chromosome 4 (**Fig. 2A**).

To corroborate our results, we looked for evidence of segmental losses of heterozygosity along chromosome 4. Eleven out of 16 sequenced diploid males bore segmental losses of heterozygosity on chromosome 4 (**Fig. 2B**). The intersection of these LOH segments comprised a 46kb peak at which all females were heterozygous, and most (11 out of 16) diploid males were homozygous. Under the CSD hypothesis, homozygosity for any allele at CSD loci permits male development. Consistently, *O. biroi* diploid males were homozygous for either allele at the 46kb region on chromosome 4 (**Table 1, supplementary fig. S2**).

The stretches of homozygosity found in diploid males could have resulted from segmental deletions resulting from improperly repaired DNA damage, or rare copy-neutral losses of heterozygosity resulting from thelytokous parthenogenesis (Kronauer et al. 2012; Oxley et al. 2014; Trible et al. 2023; Lacy et al. 2024). To distinguish between these two scenarios, we analyzed read depth and found that runs of homozygosity were not accompanied by changes in copy number (**supplementary fig. S2**). This implies that diploid males arise when rare losses of heterozygosity, which result from crossover recombination during meiosis, span the CSD locus.

Surprisingly, five of the 16 diploid males were not homozygous in this 46kb region. One possible explanation is that these individuals had mutations in other genes involved in the sex-

155 determination pathway. We therefore inspected all unique mutations and losses of heterozygosity
156 in these five diploid males, but did not find any in genes with annotated sex determining
157 functions (**supplementary file S2**). Male development may have been triggered by rare
158 stochastic perturbations to gene expression or splicing. Alternatively, these individuals may carry
159 mutations or losses of heterozygosity in genes or regulatory elements with unannotated sex
160 determination function.
161
162 The *O. biroi* CSD locus is homologous to another ant sex determination locus but not to
163 honeybee *csd*
164 To assess homology to CSD loci mapped in other species, we identified *O. biroi*
165 orthologs of the genes found in the sex determination QTL identified in *V. emeryi* (Miyakawa
166 and Mikheyev 2015) (**supplementary table S3**). This approach also identified homology to the
167 *L. humile* CSD locus, which was expected because a subset of *V.emeryiCsdQTL2* is homologous
168 to the CSD identified in *L. humile* (Pan et al. 2024). Homology to *V.emeryiCsdQTL2* was
169 scattered across one arm of *O. biroi* chromosome 4, including the 46kb CSD index peak, and
170 homology to the *L. humile* CSD locus mapped within the *O. biroi* CSD index peak (**Fig. 3A**).
171 The *O. biroi* CSD index peak contains four protein-coding genes that are also present in
172 *V.emeryiCsdQTL2*, including *HCF*, *COPA*, an uncharacterized gene, and *CRELD2*. Notably, the
173 candidate CSD region in *O. biroi* also includes a large stretch of sequence with no annotated
174 genes downstream of an uncharacterized lncRNA. LncRNAs often retain their functions and
175 synteny with surrounding genes despite divergence in sequence homology (Chodroff et al. 2010;
176 Ulitsky et al. 2011; Quinn et al. 2016), meaning that although this lncRNA has limited sequence
177 homology with *L. humile ANTSR*, it may have a homologous function (Pan et al. 2024). Because

this region is implicated in CSD in *L. humile*, our data suggest that the mechanistic basis of CSD at this locus is conserved between *O. biroi*, *L. humile*, and *V. emeryi* (**Fig. 3B**). This would mean that this sex determination locus is ancient, as these three species belong to different ant subfamilies that diverged roughly 112 million years ago (Borowiec et al. 2025).

We performed our genetic mapping in clonal line A, but different clonal lines of *O. biroi* vary in which portions of the genome are ancestrally homozygous (Oxley et al. 2014). Therefore, it was unclear whether heterozygosity at the mapped CSD locus is required for female development in all clonal lines of *O. biroi*. To investigate this, we inspected heterozygosity in diploid females from six different clonal lines by retrieving previously published genome sequences from clonal line B (Lacy et al. 2024) and sequencing genomes of diploid females from four additional clonal lines (from both the native and invasive ranges of *O. biroi* (Kronauer et al. 2012; Trible et al. 2020)). Females from all six clonal lines were heterozygous at the CSD index peak, consistent with its putative role as a CSD locus in all *O. biroi* (**Fig. 3C**).

<u>The CSD index peak has high diversity in a non-coding region.</u>

Because CSD loci are expected to evolve under balancing selection, we expect many different alleles to exist at those loci. For example, as many as 19 *csd* alleles were found to segregate in honeybee populations (Hasselmann et al. 2008), and seven alleles were found to segregate in a population of *L. humile*, despite a recent genetic bottleneck (Pan et al. 2024). Looking for elevated genetic diversity is impossible by only studying genomes from a single clonal line (i.e., asexual descendants of a single diploid female), so we looked across diploid females from six different clonal lines. We calculated nucleotide diversity (π) in 5kb sliding windows (step size = 1kb) across the genome and found a nucleotide diversity peak that fell

within the CSD index peak (**Fig. 4A, supplementary fig. S3**), between positions 1,717,00 and 1,730,000 on chromosome 4 (**Fig. 4B**).

We hypothesized that this nucleotide diversity peak resulted from many alleles found among clonal lines of *O. biroi* at this locus. Identifying these alleles requires DNA sequences of individual haplotypes, whereas short-read genome sequences of diploid females only provide diploid genotypes. To investigate allelic diversity, we retrieved previously published haploid male genome sequences from clonal lines A and B (Lacy et al. 2024) and sequenced whole genomes of haploid males from additional clonal lines. We assembled their genomes *de novo* to identify the different haplotypes found in this region. In addition to the haplotype found in the reference genome, we identified six additional haplotypes (or "alleles") in the five clonal lines for which we sequenced at least one haploid male genome (**Fig. 4C**, **Table 2**). These alleles differ substantially in their DNA sequences in the region with high nucleotide diversity (**Fig. 4C**).

To investigate which genetic elements might act to determine sex in a heterozygosity-dependent manner, we inspected all annotated genes in the CSD index peak (**Fig. 4D**). Within this region, none of the protein-coding genes contained substantial heterozygosity that affected amino acid identity (**supplementary file S3**). To determine whether any genes or exons were missing from our annotation, we performed RNA sequencing of embryos and several other life stages (including female and male adults) using several different technologies (see Methods). Briefly, we used long-read RNA sequencing (PacBio IsoSeq) to extend gene models and used several different library preparation methods followed by standard short-read (Illumina) sequencing: standard poly-A tail library prep to capture mRNAs, ribosomal RNA depletion to capture lncRNAs that are not poly-adenylated, and small RNA sequencing to annotate miRNAs,

endo-siRNAs, and putative piRNAs. Although this improved the *O. biroi* genome annotation by adding new genes and improving existing gene models (**supplementary table S4, file S4**), no new genes or exons were identified near the CSD index peak.

To look for sex-biased gene expression, we performed differential gene expression and differential transcript usage analysis between the transcriptomes of three male and three female white pupae. We used pupae for this experiment because this is the earliest life stage at which males and females can be readily distinguished. Many genes were differentially expressed between males and females (24.6% of expressed genes) or had one or more differentially used exons, including four genes near the CSD index peak (LOC105285605, LOC105283850, LOC105283849, and LOC105283844) (**supplementary tables S5 and S6; fig. S4**). However, none of these overlapped with the region of elevated genetic diversity. Very few reads aligned to the lncRNA putatively homologous to *ANTSR*, which precluded a rigorous assessment of its differential expression in *O. biroi*.

The peak of nucleotide diversity minimally affects amino acid sequences and is primarily located in a non-coding genomic region (**Fig. 4B-D**). Thus, a non-coding genetic element within this region may instruct sex determination in *O. biroi* in a heterozygosity-dependent manner. This is similar to *L. humile*, where the mapped CSD locus had high variability in non-coding and non-exonic regions (Pan et al. 2024). RNA interference of the nearby lncRNA, *ANTSR*, led to male-specific splicing of *tra*, raising the possibility that heterozygosity or homozygosity in the non-exonic and non-coding *L. humile* CSD locus affects the expression level of *ANTSR*, which instructs sex-specific splicing of *tra* (Pan et al. 2024). Because the peak of nucleotide diversity within our CSD index peak minimally affects protein-coding sequences and the region is closely

linked to a lncRNA that is putatively an ortholog of *L. humile ANTSR*, our data suggest that the mechanism of CSD in *O. biroi* may be conserved with *L. humile*.

O. biroi may have one or multiple sex determination loci.

Our CSD index mapping results suggest that *O. biroi* has a single CSD locus rather than multiple loci. However, a curious observation raises the possibility that there may be other "ghost" CSD loci that went undetected in our mapping study. We sampled many males from clonal lines A and B, and a few males from four additional clonal lines. Despite this, all the diploid males we detected came from clonal line A. We, therefore, looked back at data from previously genotyped males and found that this pattern held across a previous study (Kronauer et al. 2012). In total, from clonal line A, 22 out of 114 males were diploid, whereas all 78 males genotyped from clonal line B were haploid (**Table 3**). This disparity is statistically significant (χ^2=15.4, df=1, p<0.0001), suggesting that the two clonal lines differ in their propensity to produce diploid males.

One possible explanation for this phenomenon could be that *O. biroi* has two-locus CSD (**Fig. 1B**), but that clonal line A is ancestrally homozygous for one of the loci, whereas clonal line B retains heterozygosity at both loci. Because multi-locus CSD requires homozygosity at all sex determination loci for diploids to develop as males, in this scenario, two losses of heterozygosity would be needed for diploid males to develop in clonal line B. In contrast, only one loss of heterozygosity would be required in clonal line A, which we used for our genetic mapping.

A second QTL region identified in *V. emeryi* (*V.emeryiCsdQTL1*) contains two closely linked *tra* homologs, similar to the closely linked honeybee *tra* homologs, *csd* and *fem*. This has

led to the hypothesis that its function as a CSD locus is conserved with the *csd*-containing region of honeybees (Miyakawa and Mikheyev 2015). However, it remains to be demonstrated that either of these *tra* homologs acts as a primary CSD signal in *V. emeryi*. To test whether this locus might be involved in CSD in *O. biroi*, we searched for homology to *V.emeryiCsdQTL1* in the *O. biroi* genome and identified several regions scattered across *O. biroi* chromosome 2 (**Fig. 5A**). However, we did not find a CSD index peak on chromosome 2, and no sex determination locus with homology to the *V. emeryi* QTL was found in *L. humile* (Pan et al. 2024). Thus, the function of *V.emeryiCsdQTL1* as a primary sex determination signal might have evolved after this lineage separated from other ants (**Fig. 5B**). Alternatively, the sex determination activity of *V.emeryiCsdQTL1* could be ancestral to these three ant species and independently lost in *O. biroi* (at least in clonal line A) and *L. humile*.

Intriguingly, while clonal lines B, D, I, and M retain heterozygosity at all sites with homology to *V.emeryiQTL1* (**Fig. 5C**), clonal lines A and C are homozygous in a region homologous to a portion of *V.emeryiQTL1*. We note, however, that heterozygosity in this region is limited—it has no elevated nucleotide diversity (**supplementary fig. S3**), and there are only two nonsynonymous heterozygous variants in this region, with clonal line B conspicuously lacking any nonsynonymous heterozygosity. Therefore, it seems unlikely that this region bears a CSD locus in *O. biroi*.

Discussion

Genetically mapping sex determination loci in diverse taxa is key to understanding how sex determination evolves. Here, we investigated the mode of sex determination in the clonal raider ant, *O. biroi*. First, we mapped a sex determination locus that was heterozygous in all

females, but homozygous for either allele in diploid males (**Fig. 2**). Next, we showed that most diploid males bear rare losses of heterozygosity that arise during thelytokous parthenogenesis (**Fig. 2**). We then showed that this locus is homologous to a sex determination locus found in two other ant species—*V. emeryi* and *L. humile* (**Fig. 3**), suggesting that this mechanism of sex determination may be conserved among formicoid ants. By sequencing whole genomes of haploid males and diploid females from other clonal lines of *O. biroi,* we showed that the mapped locus corresponds to a region with high genetic diversity, following the expectation that CSD loci should evolve under balancing selection (**Fig. 4**). This diversity peaks in a noncoding genomic region, and we found limited evidence for functional heterozygosity in nearby protein-coding sequences, suggesting that heterozygosity in this noncoding sequence may trigger female development. Finally, we demonstrated that *O. biroi* CSD in clonal line A does not map to the *tra*-containing sex determination locus previously identified in *V. emeryi*, but it remains unclear whether *O. biroi* ancestrally has single-locus or multi-locus CSD (**Fig. 5**).

The presence of diploid males in many ant taxa previously led to the conclusion that most ants employ CSD (van Wilgenburg et al. 2006). Along with *L. humile* (Pan et al. 2024) and *V. emeryi* (Miyakawa and Mikheyev 2015), *O. biroi* is now one of three ant species for which heterozygosity-dependent female development has been demonstrated at mapped CSD loci. Our mapped locus appears to be homologous to *V.emeryiCsdQTL2* and to the locus identified in *L. humile* (**Fig. 3**). As was found in *L. humile*, this locus colocalizes with a peak of nucleotide diversity (**Fig. 4**), with seven alleles found among five clonal lines (**Fig. 4C, Table 2**), consistent with the expectation that CSD loci should harbor many alleles due to evolution under balancing selection. This implies that the role of this locus in CSD evolved before the divergence of the Dorylinae from the other formicoid ants roughly 112 million years ago (Borowiec et al. 2025).

Although synteny analyses raised the possibility that this locus arose early within the evolution of the Aculeata (Pan et al. 2024), genetic mapping studies of additional representative species of different ant subfamilies (especially in the poneroid clade and the Leptanillinae) and across other Aculeata will be required to determine when the function of this locus in CSD originated and how it is distributed across taxa.

In *L. humile,* a lncRNA (*ANTSR*) closely linked to this locus plays a role in sex determination (Pan et al. 2024). We did not observe substantial expression of the putative *ANTSR* homolog in *O. biroi*. This is likely because the rarity of males in *O. biroi* required us to sample males at the pupal stage, well after primary sex determination signals are transduced to self-sustaining sex-specific splicing of downstream transcription factors during the early stages of embryonic development (Gempe and Beye 2011). Therefore, we likely missed differential gene expression relevant to sex determination that occurs before the pupal stage.

We did not find a peak of the CSD index at the *O. biroi tra* homolog (**Fig. 5**), indicating that, as in *L. humile,* the mode of CSD is not homologous to the system in *A. mellifera* mediated by the *transformer* homologs *csd* and *fem*. This was previously suspected for *O. biroi* due to the presence of only a single *tra* homolog (Oxley et al. 2014) rather than the two closely linked *tra* homologs found in other ants (Privman et al. 2013). In *V. emeryi*, however, one of the two Csd QTLs (*V.emeryiCsdQTL1*) spans the *tra* locus, raising the possibility that the molecular mechanism of CSD might, in part, be conserved between *A. mellifera* and *V. emeryi* (Miyakawa and Mikheyev 2015). It has not been demonstrated that either of *V. emeryi*'s *tra* homologs act as a primary sex determination signal. Our results raise the possibility that the role of *V.emeryiCsdQTL1* as a primary sex determination signal evolved independently of *A. mellifera csd* and after *V. emeryi* diverged from *L. humile*. However, further investigations into the

mechanisms of sex determination in *V. emeryi* and other ants are required to reconstruct the evolutionary history of *V.emeryiCsdQTL1*'s function in hymenopteran sex determination.

Curiously, diploid males were only produced in clonal line A, even though many males were collected from other clonal lines (**Table 3**). One possible explanation is that *O. biroi* has multi-locus CSD, and clonal line A is ancestrally homozygous for all but one of the loci. Clonal line A is ancestrally homozygous for a portion of the region homologous to the second *V. emeryi* QTL, although it retains heterozygosity in the region overlapping *tra* (**Fig. 5C**). However, this region lacks elevated genetic diversity and functional heterozygosity, making it a poor candidate for a second CSD locus. Further study would be required to determine whether *O. biroi* has a second CSD locus. However, there may be other explanations for diploid males being found exclusively in clonal line A. For example, clonal line A could be more likely to lose heterozygosity than other clonal lines, or diploid males in clonal line A could be more likely to develop and survive. Currently, we have no data to distinguish between these hypotheses.

Another peculiarity of our study is that five of the 16 sequenced diploid males retained heterozygosity at the mapped CSD locus. Stochastic gene expression or splicing fluctuations may have caused these individuals to develop as males despite having female genotypes. Certain allelic combinations of *A. mellifera csd* trigger female development with incomplete penetrance (Beye et al. 2013), and the allelic combination found in clonal line A might similarly be permissive to occasional male development. Alternatively, these diploid males could result from mutations in or losses of heterozygosity at different genetic loci. We note that it might be easier to find rare stochastically produced diploid males in laboratory colonies of *O. biroi* than in sexual species. This is because genetically encoded diploid males only result from loss of heterozygosity, which is rare in *O. biroi* (Oxley et al. 2014; Lacy et al. 2024). By contrast, in

sexually reproducing populations, diploid males homozygous for sex determination loci will arise much more frequently due to matings between individuals that share an allele at the sex determination locus (this effect is exacerbated in invasive species like *L. humile* that have undergone recent genetic bottlenecks). Thus, if stochastically produced diploid males occur at very low baseline levels in ants, such males will rarely be detected in sexual species. In *O. biroi*, however, they could make up a substantial proportion of diploid males, simply because diploid males caused by homozygosity at the CSD locus are likewise extremely rare.

Finally, we note that heterozygosity-dependent female development, a fundamental tenet of CSD, has major implications for breeding system evolution. Due to the high fitness cost of producing sterile diploid males, species with CSD should obligatorily outbreed or have other mechanisms of maintaining heterozygosity (van Wilgenburg et al. 2006). Intriguingly, in many taxa, asexual lineages reproduce via mechanisms that lead to complete homozygosity in a single generation (Suomalainen et al. 1987; Ma and Schwander 2017). However, among the social Hymenoptera (and other Vespoids), the known modes of asexual reproduction all maintain at least some heterozygosity (Rabeling and Kronauer 2012; Ma and Schwander 2017). For formicoid ants, bees, and other taxa with CSD, asexual reproduction with high rates of heterozygosity loss would incur a steep fitness penalty due to the production of sterile diploid males. This may help explain the unusual inheritance system recently described in *O. biroi*, where following crossover recombination, reciprocally recombined chromatids are faithfully co-inherited so that no heterozygosity is lost (Lacy et al. 2024).

How this ancient putative CSD locus triggers female development in a heterozygosity-dependent manner remains unknown. In *L. humile*, RNAi experiments suggested that the expression level of the lncRNA *ANTSR* affects sex-specific splicing of *tra*, even though

384 heterozygosity in the exons of *ANTSR* is not required for this effect (Pan et al. 2024). Thus, the
385 heterozygosity-dependent function of the putative CSD locus may depend on local regulatory
386 interactions between homologous chromosomes, similar to a phenomenon known as transvection
387 (Duncan 2002). To better understand how heterozygosity induces female development in ants,
388 future studies will need to fine-map and functionally characterize this causal locus.
389
390 **Materials and Methods**
391 Software Versions
392 The versions of all software used for analyses are provided in **supplementary table S7**.
393
394 Identifying Male Ploidy
395 Clonal raider ant colonies are composed of female ants that reproduce asexually via a
396 type of thelytokous parthenogenesis termed central fusion automixis (Oxley et al. 2014). Males
397 are produced only sporadically (Oxley et al. 2014). Females of this species are diploid, whereas
398 males can either be haploid (presumably arising via a failure of central fusion following female
399 meiosis) or diploid (presumably arising due to rare losses of heterozygosity at CSD loci). Males
400 are easily recognizable due to substantial sexual dimorphism (males have eyes and wings,
401 whereas females are blind and flightless, and males also have different body shape and more
402 darkly pigmented cuticles than females). We sampled them opportunistically whenever they
403 were observed in colonies. We distinguished diploid males from haploid males based on
404 heterozygosity at several unlinked genetic markers (**supplementary table S1**). For this, we
405 disrupted one leg from each male using a Qiagen TissueLyser II and extracted DNA using
406 Qiagen's QIAmp DNA Micro Kit. We then PCR-amplified each marker and genotyped using

Sanger sequencing (for most markers) or via gel electrophoresis either after restriction digestion (for two markers) or directly after amplification (for one marker at which the different alleles are different sizes). Details of the genotyping methods can be found in **supplementary table S1**.

Genome Sequencing and Preliminary Analysis

For each library, we disrupted an individual ant with a metal bead and Qiagen's TissueLyser II and extracted DNA with Qiagen's QIAmp DNA Micro Kit. We prepared Nextera Flex Illumina DNA sequencing libraries for 16 diploid males from clonal line A, six diploid females from different clonal lines, and seven haploid males from different clonal lines. We sequenced these libraries using an Illumina NovaSeq 6000. We also accessed libraries for individual genomes from previous studies. The information for all DNA sequencing libraries used in this study can be found in **supplementary table S2**.

We trimmed reads using Trimmomatic 0.36 (Bolger et al. 2014), aligned them to the *O. biroi* reference genome (McKenzie and Kronauer 2018) (Obir_v5.4, GenBank assembly accession: GCA_003672135.1) using bwa mem (Li 2013), and then sorted, deduplicated, and indexed using picard (http://broadinstitute.github.io/picard/). We called variants using GATK HaplotypeCaller (version 4.2) (Poplin et al. 2018). To exclude falsely collapsed regions in the reference genome, we filtered against sites found to be heterozygous in haploid males. We also screened out any variants for which putatively heterozygous samples had a proportionate minor allelic depth less than 0.25 and/or for which putatively homozygous samples had a minor allelic depth greater than zero. We performed custom filtering of variants and calculated statistics using pyvcf 0.6.8 (https://github.com/jamescasbon/PyVCF), and performed sliding window analyses using pybedtools 0.9.0 (Dale et al. 2011).

430

431 CSD Index Mapping

432 By definition, CSD loci are heterozygous in females, but can be homozygous in diploid
433 males. Thus, traditional association mapping cannot identify CSD loci because particular alleles
434 do not trigger female development. Therefore, to map candidate CSD loci, we used a "CSD
435 Index," which equals zero if any female is homozygous, but if all females are heterozygous, it
436 equals the proportion of diploid males that are homozygous. Before calculating this index, we
437 had to identify ancestrally heterozygous sites. All individuals within an *O. biroi* clonal line are
438 descended asexually from a single diploid female ancestor, and CSD loci would have been
439 heterozygous in that common ancestor. Putatively ancestrally heterozygous variants are those for
440 which at least one diploid individual is heterozygous, and all other diploid individuals are either
441 heterozygous for the same two alleles, or homozygous for one of the two alleles for which other
442 diploid(s) are heterozygous (Oxley et al. 2014; Lacy et al. 2024). After identifying putatively
443 ancestrally heterozygous SNPs, we calculated the CSD index for each SNP and then recorded the
444 mean CSD index value in sliding windows.

445

446 Losses of Heterozygosity

447 We identified losses of heterozygosity as ancestrally heterozygous SNPs that had become
448 homozygous in a given sample. To assess whether homozygosity for either allele at the mapped
449 region permitted male development, we randomly chose a reference haploid male and assigned
450 allelic identity based on whether a focal sample was homozygous for the same allele or the
451 alternate allele to that possessed by the reference haploid male. To clearly illustrate losses of

heterozygosity, we used the ordinal position of SNPs rather than the position of SNPs in the reference genome assembly.

Homozygosity in whole genome sequencing data can result from deletions, for which the affected region would have half the read depth of the genome-wide average, or copy-neutral losses of heterozygosity (which result rarely from meiotic recombination and central fusion parthenogenesis (Kronauer et al. 2012; Rabeling and Kronauer 2012; Oxley et al. 2014; Lacy et al. 2024)). To determine which of these processes caused homozygosity in diploid males, we identified runs of homozygosity using "bcftools roh" (Narasimhan et al. 2016), obtained read depths at all SNPs that passed filtering within these regions using "samtools depth –aa" (Danecek et al. 2021) and then normalized by dividing by the genome-wide median read depth. For samples without losses of heterozygosity on chromosome 4, we obtained normalized read depth at all SNPs that passed filtering on chromosome 4.

Homology Between CSD Loci Across Species

To determine whether our mapped CSD locus bore homology to those identified in other ant species, we used OrthoFinder (Emms and Kelly 2019) to identify orthologs of the genes present in the two CSD QTL in *V. emeryi* (Miyakawa and Mikheyev 2015). The locus identified in *L. humile* (Pan et al. 2024) is homologous to a subset of one of the *V. emeryi* QTL. In this process, we noticed that one of the genes found within our mapped CSD locus (*cysteine-rich with EGF-like domain protein 2, or CRELD2*) was also present in a second copy in a contig that was erroneously duplicated during the genome assembly process (Chr4:21571-39095). We masked this contig and realigned sequencing data for all subsequent analyses.

475 Balancing Selection

476 Because CSD loci are expected to evolve under negative frequency-dependent
477 (balancing) selection, many different alleles should segregate in populations. To assess this, we
478 used scikit-allel (Miles et al. 2019) to calculate nucleotide diversity across six different clonal
479 lines and reported nucleotide diversity in sliding windows.

480 From inspecting DNA sequencing alignments to the reference genome, it became clear
481 that the high genetic variation within the mapped CSD locus likely resulted from several highly
482 differentiated haplotypes in this region. To investigate this further, we sequenced whole genomes
483 of haploid males from clonal lines other than A and B. We assembled the genomes of each
484 haploid male de novo using SPAdes (Bankevich et al. 2012; Prjibelski et al. 2020), found the
485 contig bearing homology to the mapped CSD locus in the reference genome assembly using
486 blastn (Camacho et al. 2009), manually scaffolded contigs as needed, and pairwise aligned each
487 alternate allele to the reference genome using nucmer and mummer (Kurtz et al. 2004) to identify
488 differences between alleles.

489

490 RNAseq for Annotation Improvements

491 To avoid missing any previously unannotated genes in the mapped CSD locus region, we
492 performed RNA sequencing following various approaches. To start, we extracted total RNA
493 from multiple samples, including separate pooled tissue from several different life stages (eggs,
494 young larvae, fourth instar larvae, prepupae, pupae, and adults), different adult tissues (antennae,
495 heads, thoraces, legs, abdomens), and individual male and female pupae using a TriZol RNA
496 extraction method followed by precipitation in isopropanol at -20C overnight. We used the
497 different life stage extractions for long read RNA-seq, rRNA depletion RNA-seq, and small

RNA-seq. We used the different adult tissues for long read RNA-seq, and the individual male and female pupae for mRNA-seq. Long read RNA-seq was performed on a PacBio Sequel II, and all other sequencing was performed on an Illumina NovaSeq 6000. For rRNA depletion, we used Illumina's TruSeq Stranded Total RNA RiboZero kit. For small RNA-seq, we prepared libraries using Perkin Elmer's NEXTFLEX Small RNA-Seq Kit v3 for Illumina Platforms.

Annotation Improvements – Long Read Transcriptome Assembly

The GenBank reference genome (GCA_003672135) for *O. biroi* (Obir_v5.4) was retrieved from NCBI in FASTA format alongside the GenBank (GCA_003672135) and RefSeq (GCF_003672135.1) transcriptomes in GTF format. Additionally, a curated RefSeq annotation was retrieved from Zenodo (https://doi.org/10.5281/zenodo.10079884) in GTF format. RefSeq assemblies were chromosome name-mapped to GenBank chromosome names using the Bioconductor GenomeInfoDb package (Arora et al. 2024) and the chromosome name maps available in NCBI.

The PacBio toolset's pbmm2 (https://github.com/PacificBiosciences/pbmm2), a PacBio wrapper for Minimap2 (Li 2018), was used for indexing and alignment of pooled full-length, non-concatemer long reads to the GenBank reference genome using the parameters "--preset ISOSEQ -j 8". Following the generation of aligned long reads in BAM format, Stringtie2 (Kovaka et al. 2019) was used with parameters "-L" for long read transcriptome assembly, and the curated RefSeq annotation was supplied as a guide for assembly using the "-G" parameter. The resulting gene models were exported for further analysis and integration as a gzipped GTF file.

Annotation Improvements – Short Read Transcriptome Assembly

For Illumina RNA-seq data, FastQ quality control was performed using Rfastp (Wang and Carroll 2024). Indexing and alignment of short reads to the GenBank genome was performed using Hisat2 (Kim et al. 2019) with default parameters, and samtools was used to generate sorted and indexed BAM files for further analysis. Stringtie2 was then used to assemble transcriptomes using the default parameters. Gene models were then combined across replicates using Stringtie2's merge function with parameters "-F 0.5 -T 2 -f 0.1" and were exported for further analysis and integration as a gzipped GTF file.

Annotation Improvements – Integrating Short and Long Read Transcriptomes with the RefSeq Assembly.

Integration of long read and short read generated gene models with the established and curated RefSeq transcriptome was performed using custom scripts in R available from GitHub (https://github.com/RockefellerUniversity/Obiroi_GeneModels_2025) and described here.

First, conflicting gene models where single long read genes map to multiple RefSeq genes and vice versa were identified. As generated long read gene models are supported by multiple full-length, non-concatemer long read alignments, attention was focused on the 720 instances of multiple long read generated genes overlapping single RefSeq genes.

Single exon long read genes were removed as these are often found to be artifacts from PacBio sequencing. Following this, long read gene models that split RefSeq gene models but matched with GenBank gene models were accepted with the corresponding RefSeq models rejected.

Next, RefSeq gene models that conflicted within themselves were removed. This includes genes that were overlapping in their exons but marked as separate genes.

After tidying RefSeq gene models, long read gene models that split RefSeq gene models but matched with short read gene models were accepted, with the corresponding RefSeq models rejected. After this gene model polishing, only 132 gene models were left where multiple long read generated genes overlapped single RefSeq genes.

To potentially rescue internally primed transcripts caused by long stretches of genomic polyAs, long read transcripts were assessed for polyA nucleotide content downstream from their endpoints, and these distributions were visualized to identify cut-offs for putative internally primed transcripts. Transcripts with at least 70 percent as 10bp downstream of the last exon or with a polyA stretch > 4 in 10bp of the last exons were labeled as putative internally primed transcripts. For putative internally primed transcripts, which also split RefSeq genes, short read gene models were used to guide the rescued models when both short read and RefSeq agreed on a single gene model.

Finally, for the remaining long read gene models that split RefSeq gene models, gaps between long read gene models were assessed in the short read and RefSeq gene models. If agreement in exon and junction structure was found between short read and RefSeq gene models, the long read gene models were rejected. This left a final 27 genes where long read gene models split RefSeq gene models, and these were manually assessed in IGV alongside short read and long read alignments to reject or accept.

With a final set of long read gene models, all RefSeq and short read transcripts that fell within single genes were then added to the long read transcriptome to create an integrated transcriptome. Duplicate transcripts were then removed from the integrated transcriptome, and

566 transcripts and genes were annotated for their sources (long read, short read, RefSeq) and any
567 overlap with the established RefSeq, GenBank, and Ensembl gene models included. Following
568 the creation of the integrated gene models, SQANTI3 (Pardo-Palacios et al. 2024) was used to
569 provide a final corrected set of gene models as well as additional QC, as described below.
570
571 Assessment of Annotation Quality and Identifying Novel Genes, Transcripts and Exons
572 SQANTI3 was run with default parameters on the integrated transcriptome against the
573 curated RefSeq and GenBank gene models to generate QC and descriptive statistics on novel and
574 non-canonical splicing events. Gffcompare software (Pertea and Pertea 2020) was run against the
575 curated RefSeq and GenBank gene models to provide statistics on novel exons, transcripts, and
576 genes.
577 BUSCO (Simão et al. 2015) was run on the integrated, curated RefSeq and GenBank
578 gene models with the parameters "-l insecta_odb10 -m tran" to provide measures of
579 transcriptome completeness based on a set of core gene models. All these metrics were
580 summarized into tables using custom R scripts available on GitHub
581 (https://github.com/RockefellerUniversity/Obiroi_GeneModels_2025).
582
583 Annotation of CDS and Functional Annotation of Genes
584 Annotation of coding regions was performed using TransDecoder (Haas 2023) to add
585 CDS information to our integrated gene models GTF. TransDecoder was run with default
586 parameters except for providing the "--single_best_only" to the TransDecoder.Predict function to
587 get only one prediction per transcript. CDS information was merged with SQANTI3's GeneMark
588 CDS annotation for a final set of CDSs. With this coding information, gene models were read

into R, translated into protein sequences using the BioStrings package, and protein per transcript sequences exported as FASTA format for use in downstream tools. For functional annotation, both eggNOG (Huerta-Cepas et al. 2019) and InterProScan (Jones et al. 2014) were used using default parameters with our protein sequences FASTA to provide predictions for functional annotations of genes including their putative GO, KEGG, PFAM and Panther categories. Annotations were summarized to gene levels from transcript level annotation using R.

Annotation of lncRNAs

FEELnc (Wucher et al. 2017) was used to identify putative lncRNAs within our final integrated gene models. First, the FEELnc_filter.pl script was run with default parameters, and then the FEELnc_codpot.pl script was run with parameters "--mode=shuffle" to generate our putative set of lncRNAs for annotation of our integrated gene model GTF.

Annotation of miRNAs

Small RNA-seq reads were adaptor clipped for a "TGGAATTCTCGGGTGCCAAGG" adapter using CLIPflexR (Rozen-Gagnon et al. 2021) and aligned to the genome using miRDeep2's mapper.pl script with parameters "-c -j -m -l 18" (Friedländer et al. 2012). Aligned data were then processed using miRDeep2's miRDeep2.pl script with a FASTA of known *Drosophila* miRNAs retrieved from miRBase (Kozomara et al. 2019). The resulting annotated miRNA genomic locations were merged across samples and added into our integrated gene model GTF.

Annotation of piRNAs

For the identification of piRNA clusters, small read RNA-seq was processed using the pipeline workflow described within the Pilfer (Ray and Pandey 2018) toolkit to generate piRNA cluster BED files per sample. The sample piRNA clusters were then merged across samples to produce a final piRNA cluster set, which was then included in our integrated gene model GTF.

Annotation of tRNAs, snRNAs, snoRNAs and rRNAs

Additional annotations for tRNAs, snRNAs, snoRNAs and rRNAs were mapped from RefSeq annotation onto our integrated gene model GTF.

Sex-specific Gene Expression

To identify genes with sex-specific expression, we aligned Illumina mRNA-seq reads from three female and three male pupae using STAR (v2.5.0a) (Dobin et al. 2013). We counted and assigned reads to genes and transcripts using RSEM (v1.2.28) (Li and Dewey 2011). We analyzed differential gene expression using DESeq2 (Love et al. 2014), filtering out genes shorter than ten bases or with less than ten counts across all six samples. We hierarchically clustered the differentially expressed genes by Euclidian distance using the R package pheatmap (v1.0.12) (Kolde 2024). We used DEXSeq (v1.50.0) (Anders et al. 2012) to identify differential exon usage.

Data and Software Availability

All DNA and RNA sequencing data are publicly available at the National Center for Biotechnology Information Sequence Read Archive under accession number PRJNA1075055. All other data are available in the article and Supporting Information. All code is available on

GitHub (genome annotation: https://github.com/RockefellerUniversity/Obiroi_GeneModels_2025; differential gene expression and exon usage: https://github.com/jina-leemon/CSD_biroi_male-female-RNA-seq; all other code and analyses: https://github.com/kipdlacy/SexDetermination_Obiroi).

Contributions

K.D.L., J.L., and D.J.C.K. designed research; J.L. analyzed data and visualized results for gene-expression and exon usage analyses; K.R.G., W.W., and T.C. improved the genome annotation with input from K.D.L.; K.D.L. performed research, analyzed data, and visualized results for all other parts of the manuscript; K.D.L. and D.J.C.K. wrote the manuscript; D.J.C.K. supervised the project.

Competing interests

The authors declare no competing interests.

Acknowledgements

We thank Stephany Valdés-Rodríguez, Leonora Olivos-Cisneros, Alejandra Hurtado-Giraldo, Sean McKenzie, and other members of the Kronauer laboratory for helping us obtain male ants and for valuable discussions; Jenn Balacco and the Rockefeller University Reference Genome Resource Center for long read RNA sequencing; the Weill Cornell Genomics Resources Core Facility for Small RNA sequencing; Connie Zhao and the Rockefeller University Genomics Resource Center for rRNA-depletion sequencing and all other Illumina sequencing; Tom Kay, Matteo Rossi, and Yukina Chiba for valuable comments on an earlier version of the manuscript.

This work was supported by a Gabrielle H. Reem and Herbert J. Kayden Early-Career Innovation Award and the National Institute of General Medical Sciences of the National Institutes of Health under award no. R35GM127007, both to D.J.C.K. The content is solely the responsibility of the authors and does not necessarily represent the official views of the National Institutes of Health. This work was also supported by the Howard Hughes Medical Institute, where D.J.C.K. is an Investigator. This is Clonal Raider Ant Project paper number 36.

References

Anders S, Reyes A, Huber W. 2012. Detecting differential usage of exons from RNA-seq data. *Genome Research* 22:2008–2017.

Arora S, Morgan M, Carlson M, Pagès H. 2024. GenomeInfoDb: Utilities for manipulating chromosome names, including modifying them to follow a particular naming style.

Bachtrog D, Mank JE, Peichel CL, Kirkpatrick M, Otto SP, Ashman TL, Hahn MW, Kitano J, Mayrose I, Ming R, et al. 2014. Sex determination: why so many ways of doing it? *PLoS Biology* 12:e1001899.

Bankevich A, Nurk S, Antipov D, Gurevich AA, Dvorkin M, Kulikov AS, Lesin VM, Nikolenko SI, Pham S, Prjibelski AD, et al. 2012. SPAdes: a new genome assembly algorithm and its applications to single-cell sequencing. *Journal of Computational Biology* 19:455–477.

Beye M, Hasselmann M, Fondrk MK, Page RE, Omholt SW. 2003. The gene *csd* is the primary signal for sexual development in the honeybee and encodes an SR-type protein. *Cell* 114:419–429.

Beye M, Seelmann C, Gempe T, Hasselmann M, Vekemans X, Fondrk MK, Page RE. 2013. Gradual molecular evolution of a sex determination switch through incomplete penetrance of femaleness. *Current Biology* 23:2559–2564.

Bolger AM, Lohse M, Usadel B. 2014. Trimmomatic: a flexible trimmer for Illumina sequence data. *Bioinformatics* 30:2114–2120.

Bopp D;, Saccone G;, Beye M. 2014. Sex determination in insects: variations on a common theme. *Sexual Development* 8:20–28.

Borowiec ML, Rabeling C, Brady SG, Fisher BL, Schultz TR, Ward PS. 2019. Compositional heterogeneity and outgroup choice influence the internal phylogeny of the ants. *Molecular Phylogenetics and Evolution* 134:111–121.

689 Borowiec ML, Zhang YM, Neves K, Ramalho MO, Fisher BL, Lucky A, Moreau CS. 2025.
690 Evaluating UCE data adequacy and integrating uncertainty in a comprehensive
691 phylogeny of ants. *Systematic Biology*:syaf001.

692 Camacho C, Coulouris G, Avagyan V, Ma N, Papadopoulos J, Bealer K, Madden TL. 2009.
693 BLAST+: architecture and applications. *BMC Bioinformatics* 10:1–9.

694 Chodroff RA, Goodstadt L, Sirey TM, Oliver PL, Davies KE, Green ED, Molnár Z, Ponting CP.
695 2010. Long noncoding RNA genes: conservation of sequence and brain expression
696 among diverse amniotes. *Genome Biology* 11:R72.

697 Crozier RH. 1971. Heterozygosity and sex determination in haplo-diploidy. *The American*
698 *Naturalist* 105:399–412.

699 Dale RK, Pedersen BS, Quinlan AR. 2011. Pybedtools: a flexible Python library for
700 manipulating genomic datasets and annotations. *Bioinformatics* 27:3423–3424.

701 Danecek P, Bonfield JK, Liddle J, Marshall J, Ohan V, Pollard MO, Whitwham A, Keane T,
702 McCarthy SA, Davies RM, et al. 2021. Twelve years of SAMtools and BCFtools.
703 *GigaScience* 10:giab008.

704 Dobin A, Davis CA, Schlesinger F, Drenkow J, Zaleski C, Jha S, Batut P, Chaisson M, Gingeras
705 TR. 2013. STAR: ultrafast universal RNA-seq aligner. *Bioinformatics* 29:15–21.

706 Duncan IW. 2002. Transvection effects in *Drosophila*. *Annual Review of Genetics* 36:521–556.

707 Emms DM, Kelly S. 2019. OrthoFinder: phylogenetic orthology inference for comparative
708 genomics. *Genome Biology* 20:238.

709 Friedländer MR, Mackowiak SD, Li N, Chen W, Rajewsky N. 2012. miRDeep2 accurately
710 identifies known and hundreds of novel microRNA genes in seven animal clades. *Nucleic*
711 *Acids Research* 40:37–52.

712 Gempe T, Beye M. 2011. Function and evolution of sex determination mechanisms, genes and
713 pathways in insects. *BioEssays* 33:52–60.

714 Gempe T, Hasselmann M, Schiøtt M, Hause G, Otte M, Beye M. 2009. Sex determination in
715 honeybees: Two separate mechanisms induce and maintain the female pathway. *PLoS*
716 *Biology* 7:e1000222.

717 Haas B. 2023. TransDecoder (find coding regions within transcripts). Available from:
718 https://github.com/TransDecoder/TransDecoder

719 Hasselmann M, Beye M. 2004. Signatures of selection among sex-determining alleles of the
720 honey bee. *Proceedings of the National Academy of Sciences* 101:4888–4893.

721 Hasselmann M, Gempe T, Schiøtt M, Nunes-Silva CG, Otte M, Beye M. 2008. Evidence for the
722 evolutionary nascence of a novel sex determination pathway in honeybees. *Nature*
723 454:519–522.

724 Huerta-Cepas J, Szklarczyk D, Heller D, Hernández-Plaza A, Forslund SK, Cook H, Mende DR,
725 Letunic I, Rattei T, Jensen LJ, et al. 2019. eggNOG 5.0: a hierarchical, functionally and
726 phylogenetically annotated orthology resource based on 5090 organisms and 2502
727 viruses. *Nucleic Acids Research* 47:D309–D314.

728 Jones P, Binns D, Chang H-Y, Fraser M, Li W, McAnulla C, McWilliam H, Maslen J, Mitchell
729 A, Nuka G, et al. 2014. InterProScan 5: genome-scale protein function classification.
730 *Bioinformatics* 30:1236–1240.

731 Kim D, Paggi JM, Park C, Bennett C, Salzberg SL. 2019. Graph-based genome alignment and
732 genotyping with HISAT2 and HISAT-genotype. *Nature Biotechnology* 37:907–915.

733 Kolde R. 2024. pheatmap: Pretty Heatmaps. Available from:
734 https://github.com/raivokolde/pheatmap

735 Kovaka S, Zimin AV, Pertea GM, Razaghi R, Salzberg SL, Pertea M. 2019. Transcriptome
736 assembly from long-read RNA-seq alignments with StringTie2. *Genome Biology* 20:278.

737 Kozomara A, Birgaoanu M, Griffiths-Jones S. 2019. miRBase: from microRNA sequences to
738 function. *Nucleic Acids Research* 47:D155–D162.

739 Kronauer DJC, Pierce NE, Keller L. 2012. Asexual reproduction in introduced and native
740 populations of the ant *Cerapachys biroi*. *Molecular Ecology* 21:5221–5235.

741 Kurtz S, Phillippy A, Delcher AL, Smoot M, Shumway M, Antonescu C, Salzberg SL. 2004.
742 Versatile and open software for comparing large genomes. *Genome Biology* 5:R12.

743 Lacy KD, Hart T, Kronauer DJC. 2024. Co-inheritance of recombined chromatids maintains
744 heterozygosity in a parthenogenetic ant. *Nature Ecology & Evolution* 8:1522–1533.

745 Li B, Dewey CN. 2011. RSEM: accurate transcript quantification from RNA-Seq data with or
746 without a reference genome. *BMC Bioinformatics* 12:323.

747 Li H. 2013. Aligning sequence reads, clone sequences and assembly contigs with BWA-MEM.
748 Available from: http://arxiv.org/abs/1303.3997

749 Li H. 2018. Minimap2: pairwise alignment for nucleotide sequences. *Bioinformatics* 34:3094–
750 3100.

751 Love MI, Huber W, Anders S. 2014. Moderated estimation of fold change and dispersion for
752 RNA-seq data with DESeq2. *Genome Biology* 15:550.

753 Ma W-J, Schwander T. 2017. Patterns and mechanisms in instances of endosymbiont□induced
754 parthenogenesis. *Journal of Evolutionary Biology* 30:868–888.

Matthey-Doret C, van der Kooi CJ, Jeffries DL, Bast J, Dennis AB, Vorburger C, Schwander T. 2019. Mapping of multiple complementary sex determination loci in a parasitoid wasp. *Genome Biology and Evolution* 11:2954–2962.

McKenzie SK, Kronauer DJC. 2018. The genomic architecture and molecular evolution of ant odorant receptors. *Genome Research* 28:1757–1765.

Miles A, Ralph P, Rae S, Pisupati R. 2019. cggh/scikit-allel: v1.2.1. Available from: https://zenodo.org/records/3238280

Miyakawa MO, Mikheyev AS. 2015. QTL mapping of sex determination loci supports an ancient pathway in ants and honey bees. *PLoS Genetics* 11:e1005656.

Miyakawa MO, Miyakawa H. 2023. *Transformer* gene regulates feminization under two complementary sex determination loci in the ant, *Vollenhovia emeryi*. *Insect Biochemistry and Molecular Biology* 156:103938.

Miyakawa MO, Tsuchida K, Miyakawa H. 2018. The doublesex gene integrates multi-locus complementary sex determination signals in the Japanese ant, *Vollenhovia emeryi*. *Insect Biochemistry and Molecular Biology* 94:42–49.

Narasimhan V, Danecek P, Scally A, Xue Y, Tyler-Smith C, Durbin R. 2016. BCFtools/RoH: a hidden Markov model approach for detecting autozygosity from next-generation sequencing data. *Bioinformatics* 32:1749–1751.

Normark BB. 2003. The evolution of alternative genetic systems in insects. *Annual Review of Entomology* 48:397–423.

Otte M, Netschitailo O, Weidtkamp-Peters S, Seidel CAM, Beye M. 2023. Recognition of polymorphic Csd proteins determines sex in the honeybee. *Science Advances* 9:eadg4239.

Oxley PR, Ji L, Fetter-Pruneda I, McKenzie SK, Li C, Hu H, Zhang G, Kronauer DJC. 2014. The genome of the clonal raider ant *Cerapachys biroi*. *Current Biology* 24:451–458.

Pan Q, Darras H, Keller L. 2024. LncRNA gene ANTSR coordinates complementary sex determination in the Argentine ant. *Science Advances* 10:eadp1532.

Pardo-Palacios FJ, Arzalluz-Luque A, Kondratova L, Salguero P, Mestre-Tomás J, Amorín R, Estevan-Morió E, Liu T, Nanni A, McIntyre L, et al. 2024. SQANTI3: curation of long-read transcriptomes for accurate identification of known and novel isoforms. *Nature Methods* 21:793–797.

Pertea G, Pertea M. 2020. GFF Utilities: GffRead and GffCompare. Available from: https://f1000research.com/articles/9-304

Poplin R, Ruano-Rubio V, DePristo MA, Fennell TJ, Carneiro MO, Auwera GAV der, Kling DE, Gauthier LD, Levy-Moonshine A, Roazen D, et al. 2018. Scaling accurate genetic

variant discovery to tens of thousands of samples. Available from: https://www.biorxiv.org/content/10.1101/201178v3

Privman E, Wurm Y, Keller L. 2013. Duplication and concerted evolution in a master sex determiner under balancing selection. *Proceedings of the Royal Society B: Biological Sciences* 280:20122968.

Prjibelski A, Antipov D, Meleshko D, Lapidus A, Korobeynikov A. 2020. Using SPAdes De Novo Assembler. *Current Protocols in Bioinformatics* 70:e102.

Quinn JJ, Zhang QC, Georgiev P, Ilik IA, Akhtar A, Chang HY. 2016. Rapid evolutionary turnover underlies conserved lncRNA–genome interactions. *Genes & Development* 30:191–207.

Rabeling C, Kronauer DJC. 2012. Thelytokous parthenogenesis in eusocial Hymenoptera. *Annual Review of Entomology* 58:273–292.

Ray R, Pandey P. 2018. piRNA analysis framework from small RNA-Seq data by a novel cluster prediction tool - PILFER. *Genomics* 110:355–365.

Rozen-Gagnon K, Gu M, Luna JM, Luo J-D, Yi S, Novack S, Jacobson E, Wang W, Paul MR, Scheel TKH, et al. 2021. Argonaute-CLIP delineates versatile, functional RNAi networks in *Aedes aegypti*, a major vector of human viruses. *Cell Host & Microbe* 29:834–848.

Seiler J, Beye M. 2024. Honeybees' novel complementary sex-determining system: function and origin. *Trends in Genetics* 40:969–981.

Simão FA, Waterhouse RM, Ioannidis P, Kriventseva EV, Zdobnov EM. 2015. BUSCO: assessing genome assembly and annotation completeness with single-copy orthologs. *Bioinformatics* 31:3210–3212.

Suomalainen E, Saura A, Lokki J. 1987. Cytology and Evolution in Parthenogenesis. CRC Press

Trible W, Chandra V, Lacy KD, Limón G, McKenzie SK, Olivos-Cisneros L, Arsenault SV, Kronauer DJC. 2023. A caste differentiation mutant elucidates the evolution of socially parasitic ants. *Current Biology* 33:1047–1058.

Trible W, Mckenzie SK, Kronauer DJC. 2020. Globally invasive populations of the clonal raider ant are derived from Bangladesh. *Biology Letters* 16:20200105.

Ulitsky I, Shkumatava A, Jan CH, Sive H, Bartel DP. 2011. Conserved function of lincRNAs in vertebrate embryonic development despite rapid sequence evolution. *Cell* 147:1537–1550.

Verhulst EC, Beukeboom LW, van de Zande L. 2010. Maternal control of haplodiploid sex determination in the wasp *Nasonia*. *Science* 328:620–623.

Wang W, Carroll T. 2024. Rfastp: An ultra-fast and all-in-one fastq preprocessor (quality control, adapter, low quality and polyX trimming) and UMI sequence parsing). Available from: 10.18129/B9.bioc.Rfastp

Wexler J, Delaney EK, Belles X, Schal C, Wada-Katsumata A, Amicucci MJ, Kopp A. 2019. Hemimetabolous insects elucidate the origin of sexual development via alternative splicing. *eLife* 8:e47490.

Whiting PW. 1933. Selective fertilization and sex-determination in Hymenoptera. *Science* 78:537–538.

Whiting PW. 1935. Genic balance, sex-determination and selective fertilization in Hymenoptera. *Proceedings of the American Philosophical Society* 75:517–520.

Whiting PW. 1943. Multiple alleles in complementary sex determination of *Habrobracon*. *Genetics* 28:365–382.

van Wilgenburg E, Driessen G, Beukeboom LW. 2006. Single locus complementary sex determination in Hymenoptera: an “unintelligent” design? *Frontiers in Zoology* 3:1.

Williams TM, Carroll SB. 2009. Genetic and molecular insights into the development and evolution of sexual dimorphism. *Nature Reviews Genetics* 10:797–804.

Wucher V, Legeai F, Hédan B, Rizk G, Lagoutte L, Leeb T, Jagannathan V, Cadieu E, David A, Lohi H, et al. 2017. FEELnc: a tool for long non-coding RNA annotation and its application to the dog transcriptome. *Nucleic Acids Research* 45:e57.

Zou Y, Geuverink E, Beukeboom LW, Verhulst EC, van de Zande L. 2020. A chimeric gene paternally instructs female sex determination in the haplodiploid wasp *Nasonia*. *Science* 370:1115–1118.

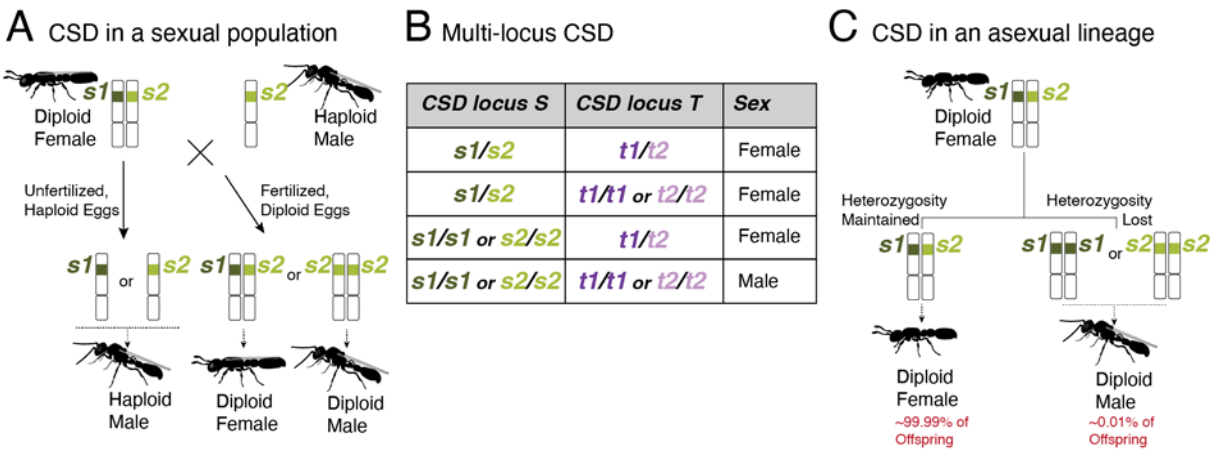

CSD locus S	CSD locus T	Sex
s1/s2	t1/t2	Female
s1/s2	t1/t1 or t2/t2	Female
s1/s1 or s2/s2	t1/t2	Female
s1/s1 or s2/s2	t1/t1 or t2/t2	Male

Fig. 1. Theoretical expectations for complementary sex determination (CSD). (A) Cartoon depicting a mating between a diploid female with two different alleles at a sex determination locus and a haploid male bearing one of these two alleles. Half of the sexually produced diploid offspring are expected to develop as males. **(B)** Table illustrating multi-locus CSD in diploids, in which heterozygosity of at least one sex determination locus is required for female development. By contrast, only homozygosity at all loci results in diploid male development. **(C)** Cartoon depicting how CSD might work in asexual species such as the clonal raider ant. If diploid males arise from losses of heterozygosity at sex loci, then homozygosity for either of the two alleles should trigger male development. Offspring proportions reflect empirical observations in the clonal raider ant (Kronauer et al. 2012; Oxley et al. 2014).

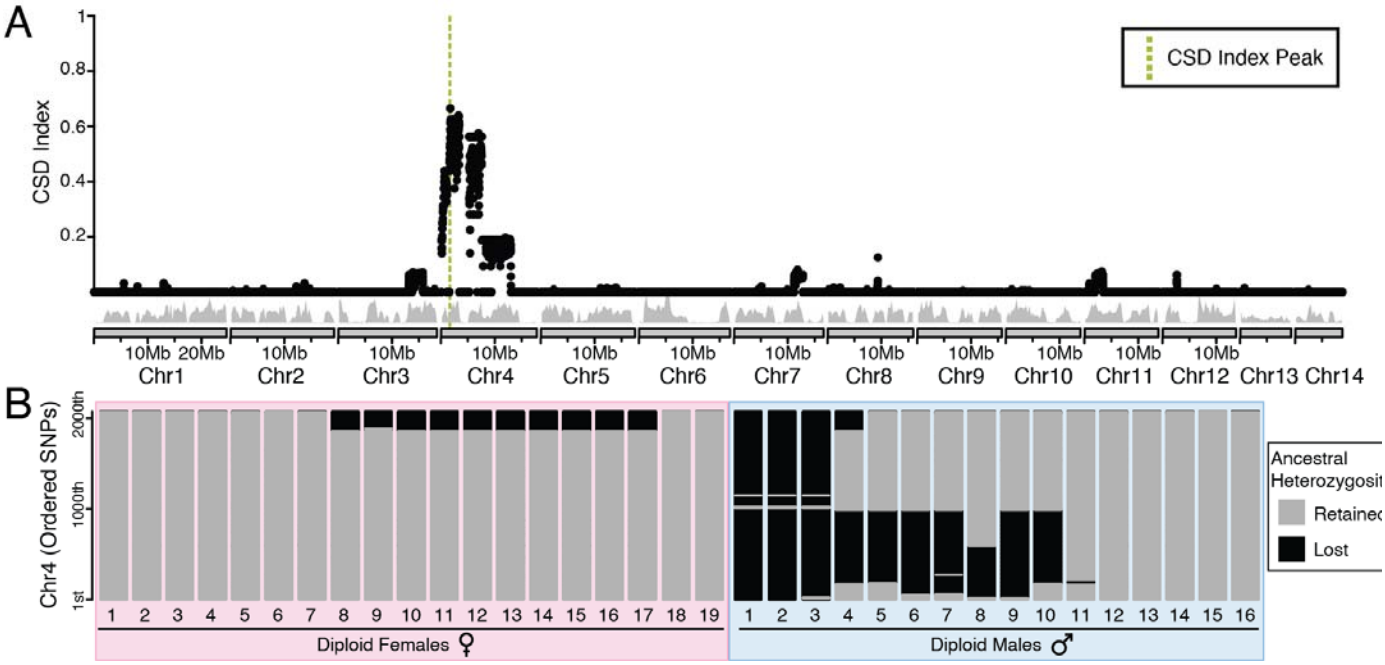

Fig. 2. Whole genome sequencing reveals a candidate sex determination locus on chromosome 4. (A) Karyoplot depicting the mean CSD index in 50kb windows with a 15kb sliding interval. For each SNP, the CSD index equals zero if any female is homozygous. If all females are heterozygous, the CSD index equals the proportion of homozygous diploid males. The CSD index peak is shown as a green dotted line. The grey histogram shows the number of ancestrally heterozygous SNPs in 200kb windows. **(B)** Stacked bar plots for all diploids used for mapping, with one horizontal line for each ordered putatively ancestrally heterozygous SNP on chromosome 4. For each sample, SNPs that retain ancestral heterozygosity are drawn as grey lines, whereas SNPs that have lost ancestral heterozygosity are drawn as black lines.

	Heterozygous	**Homozygous Allele 1**	**Homozygous Allele 2**
Diploid Females	19	0	0
Diploid Males	5	2	9

865 **Table 1.** Number of samples heterozygous and homozygous for each allele in the 46kb region on

866 chromosome 4.

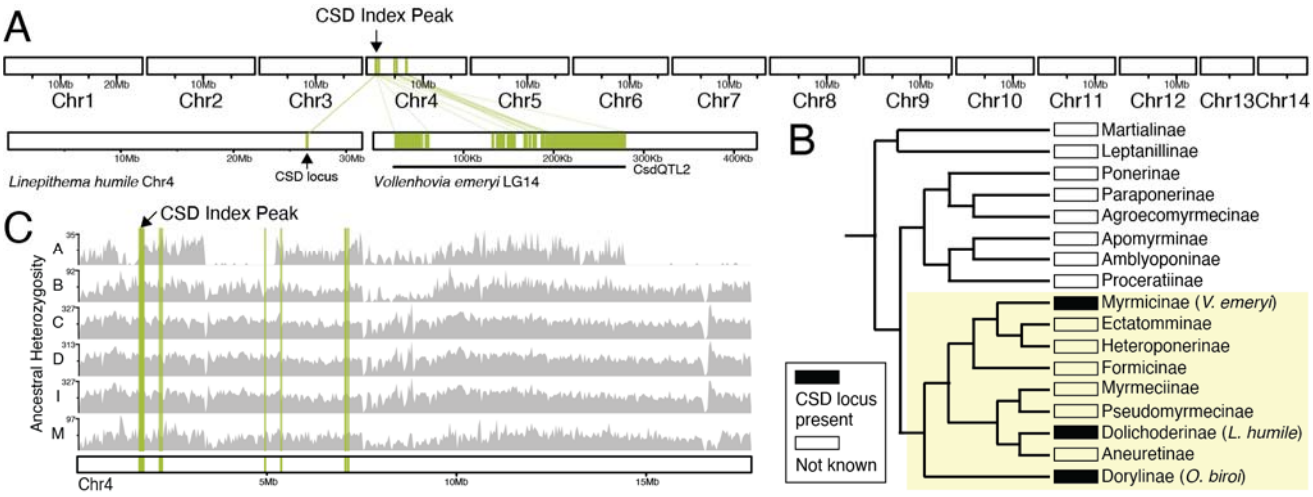

867

868 **Fig. 3. The putative sex determination locus identified in *O. biroi* is conserved across formicoid ants.**

869 **(A)** Karyoplot depicting the 14 chromosomes in the *O. biroi* genome, chromosome 4 from the *L. humile*

870 genome (Pan et al. 2024), and one contig from linkage group 14 of the *V. emeryi* reference genome

871 (Miyakawa and Mikheyev 2015). Note that the plots from the different species are not drawn to scale.

872 Homology to protein-coding genes identified within *V.emeryiCsdQTL2* is drawn in green. The location of

873 the *O. biroi* CSD index peak is indicated. **(B)** A phylogeny of the ant subfamilies (adapted from

874 (Borowiec et al. 2019)), with the presence of a sex determination locus homologous to the peak of our

875 CSD index, or the absence of data shown. The yellow shaded background denotes the formicoid clade.

876 **(C)** Karyoplot for *O. biroi* chromosome 4, depicting homology to *V.emeryiCsdQTL2* and ancestral

877 heterozygosity for six different clonal lines (A, B, C, D, I, and M). Grey histograms depict the number of

878 ancestrally heterozygous SNPs in 100kb windows.

879

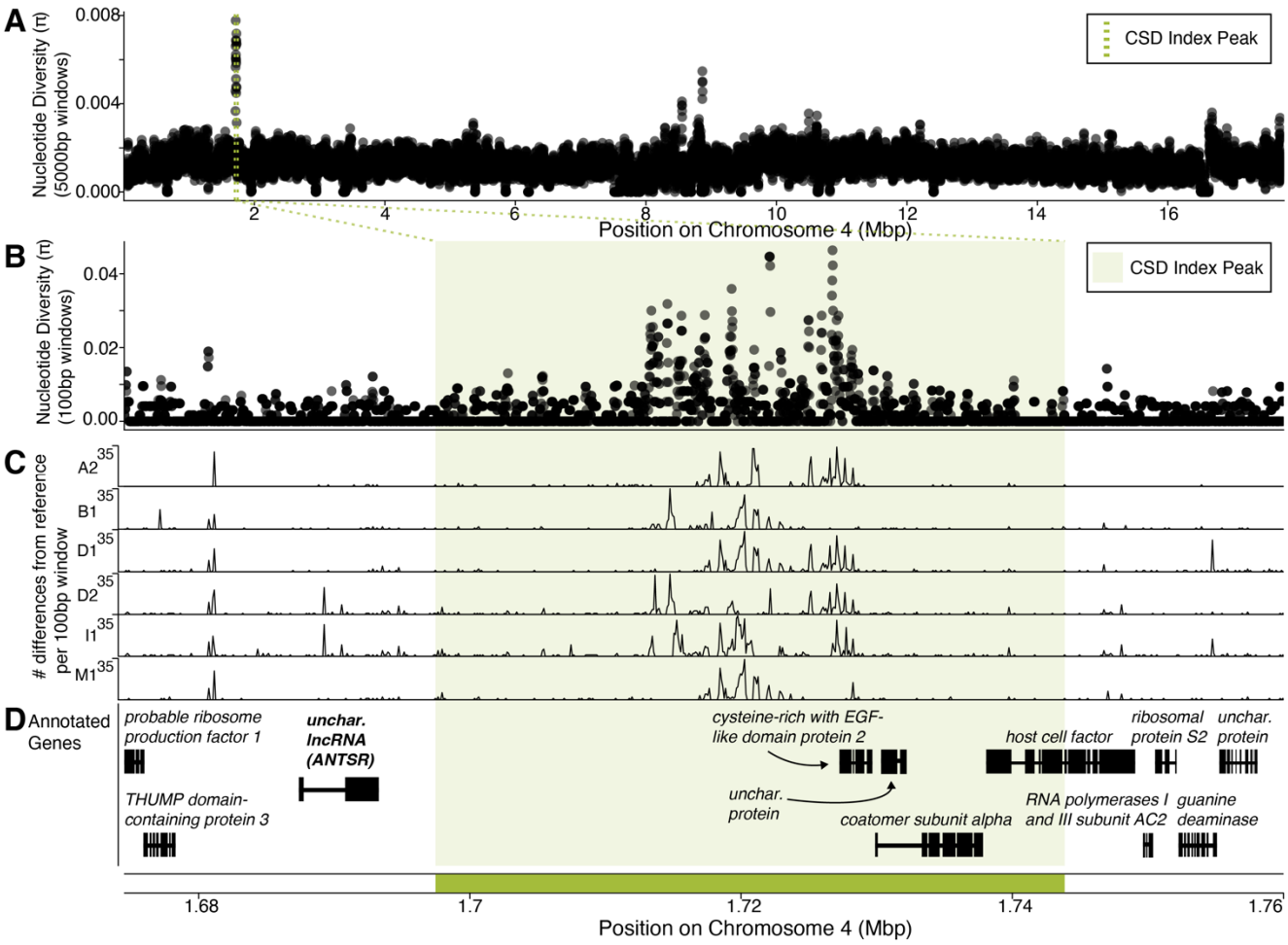

<u>Fig. 4.</u> The CSD index peak is characterized by high genetic diversity in a non-coding region. (A & B) Nucleotide diversity across the length of *O. biroi* chromosome 4 in 5kb windows (step size=1kb) **(A)** and across the vicinity of the CSD index peak in 100bp windows (step size=20bp) **(B)**. **(C)** The number of differences per 100bp window between each alternate *de novo* assembled allele and the reference genome allele. **(D)** Annotated genes in the vicinity of the CSD index peak. Black boxes depict exons and thin lines depict introns. The lncRNA *ANTSR* is indicated in bold. Arrows indicate the names of genes in close proximity. The CSD index peak is shown as a green dotted line in A, and with green shading in B-D.

Clonal Line	**CSD Index Peak Haplotypes**
A	A1 / A2
B	B1 / A1
C	? / ?
D	D1 / D2
I	I1 / ?
M	M1 / A1

888 **Table 2.** The haplotypes present at the CSD index peak for each studied *O. biroi* clonal line.

Clonal Line	**Haploid Males**	**Diploid Males**
A	92	22
B	78	0
C	6	0
D	4	0
I	1	0
M	2	0

889 **Table 3.** Number of haploid and diploid males sampled from different *O. biroi* clonal lines.

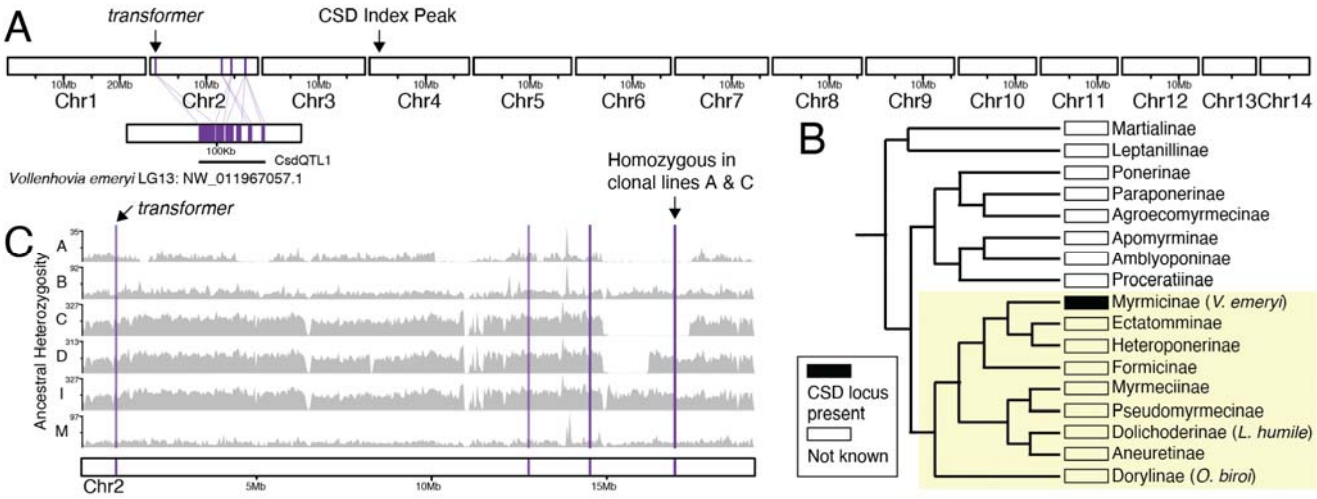

Fig. 5. Whether a second, *tra*-containing CSD QTL from *V. emeryi* is conserved across ants remains ambiguous. (A) Karyoplot depicting the 14 chromosomes in the *O. biroi* genome and one contig from linkage group 13 of the *V. emeryi* reference genome. Homology to protein-coding genes identified within *V.emeryiCsdQTL1* is drawn in purple. The locations of the *O. biroi* CSD index peak and the homolog of *transformer* are indicated. **(B)** A phylogeny of the ant subfamilies (adapted from (Borowiec et al. 2019)), with the presence or absence of this second putative sex determination locus, or the absence of data shown. The yellow shaded background denotes the formicoid clade. **(C)** Karyoplot for *O. biroi* chromosome 2, depicting homology to *V.emeryiCsdQTL1* and ancestral heterozygosity for each clonal line. Grey histograms depict the number of ancestrally heterozygous SNPs in 100kb windows. The region of homology that is ancestrally homozygous in clonal lines A and C is labeled.

901 **Supplementary Figures**

902

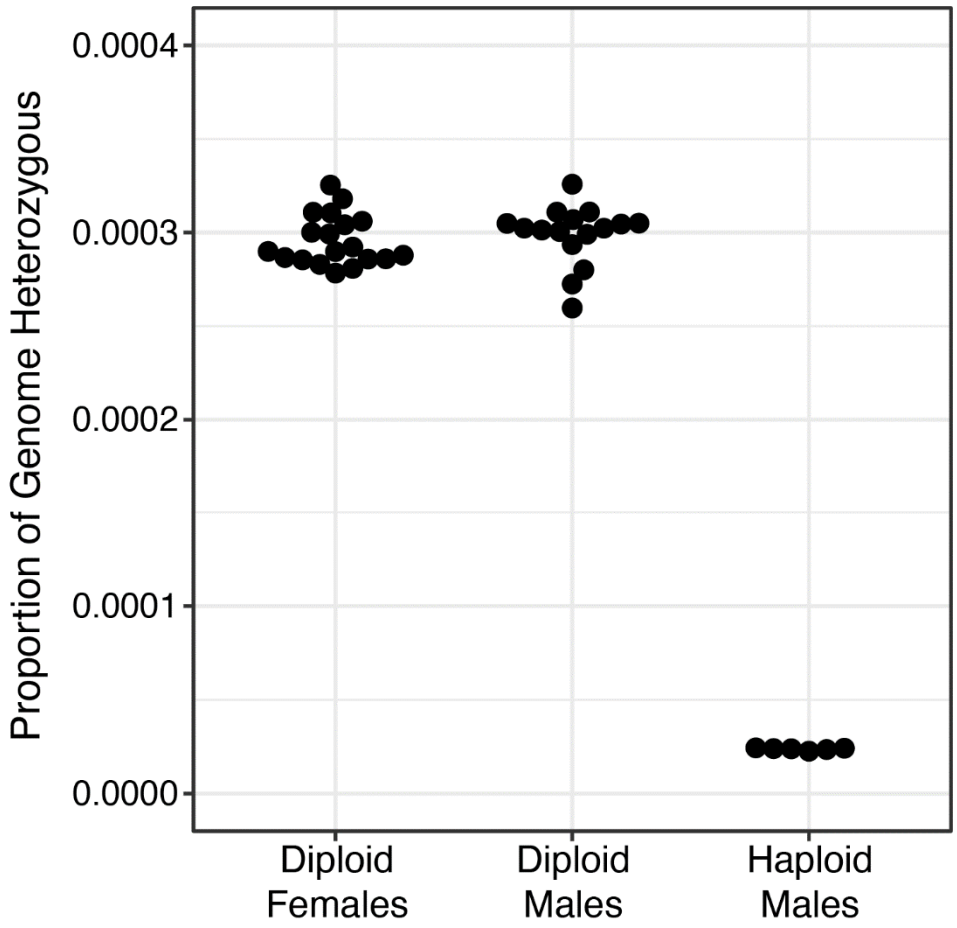

903

904 **Supplementary Fig. S1. Genome-wide heterozygosity levels.** Scatterplot depicting the

905 proportion of base pairs in the ~220Mb *O. biroi* genome that are heterozygous in each individual

906 for which we conducted whole genome sequencing. Haploid males have no legitimate

907 heterozygosity—the small elevation above zero is due to heterozygous genotype calls at

908 erroneously assembled regions of the reference genome.

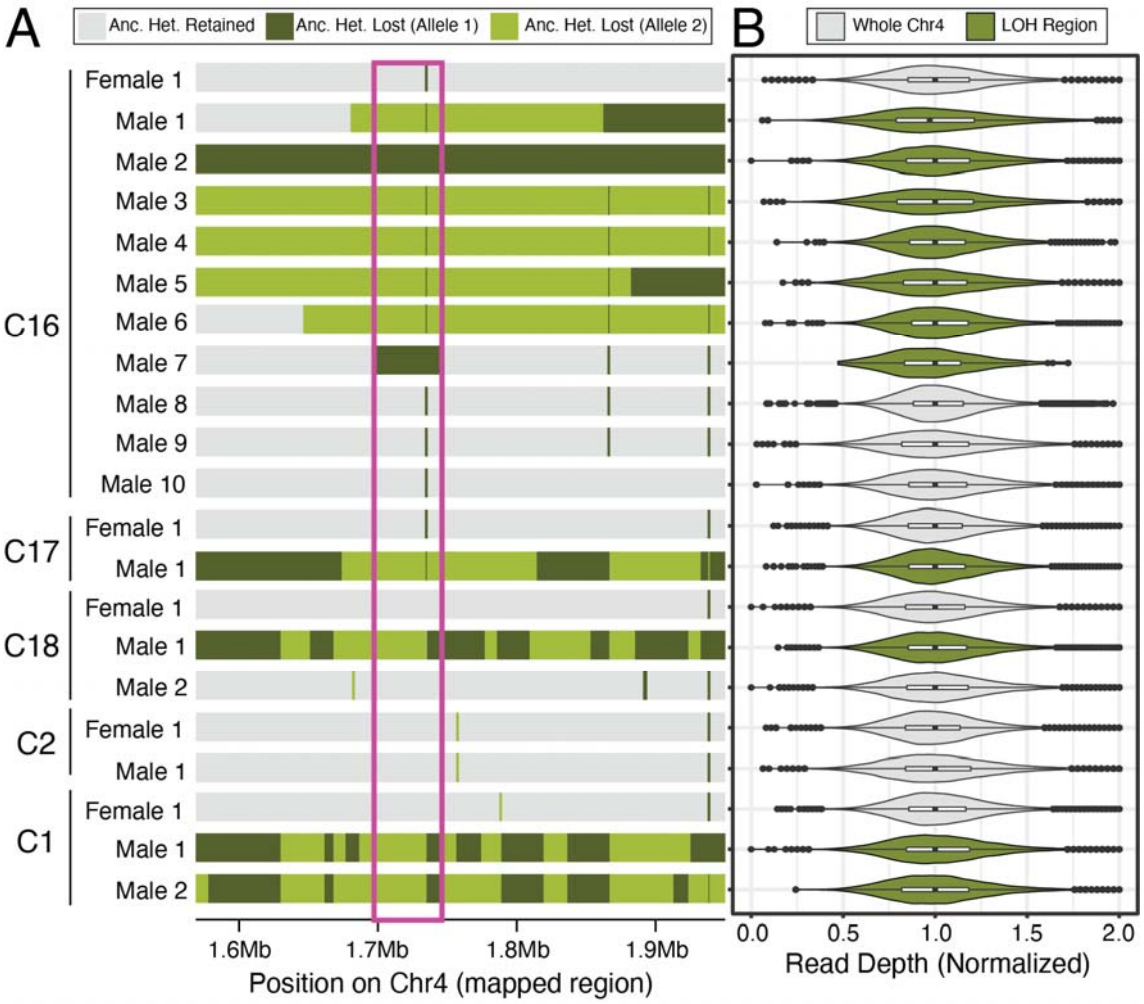

<u>Supplementary Fig. S2.</u> Diploid males result from copy-neutral losses of heterozygosity for either allele. (A) Karyoplot depicting losses (green) or retention (gray) of heterozygosity across the vicinity of the peak of the CSD index in diploid males and females. Codes at the left (C16, C17, etc.) indicate the stock colonies from which each ant was sampled. The magenta box surrounds the CSD index peak. Dark green indicates that the sample has the same allele / haplotype as the reference haploid male whereas light green indicates that the sample has the alternative allele. Switches between alleles in homozygous regions within samples (i.e., changes from light green to dark green or vice versa) represent recombination events that occurred in generations prior to the meiosis that produced each diploid male. Because the reference haploid

male was from colony C16, fewer generations have elapsed since the common ancestor of the reference haploid male and the diploid males from that colony, and thus fewer recombination events have accumulated. By contrast, more generations have elapsed since the common ancestor of the reference haploid male and the diploid males from colonies C17, C18, and C1, which is reflected in the higher number of recombination events that accumulated across generations. **(B)** Normalized read depth across either all SNPs that passed filtering on chromosome 4 (gray, for samples without losses of heterozygosity on chromosome 4) or all SNPs that passed filtering within that sample's loss of heterozygosity region (green). Box plots show median (center line), interquartile range (IQR) (box limits) and 1.5 x IQR (whiskers). Data points that fall outside 1.5 x IQR are shown individually. Violin plots show the kernel probability density, meaning that the proportion of the data located at an x-axis value is represented by the width of the outlined area.

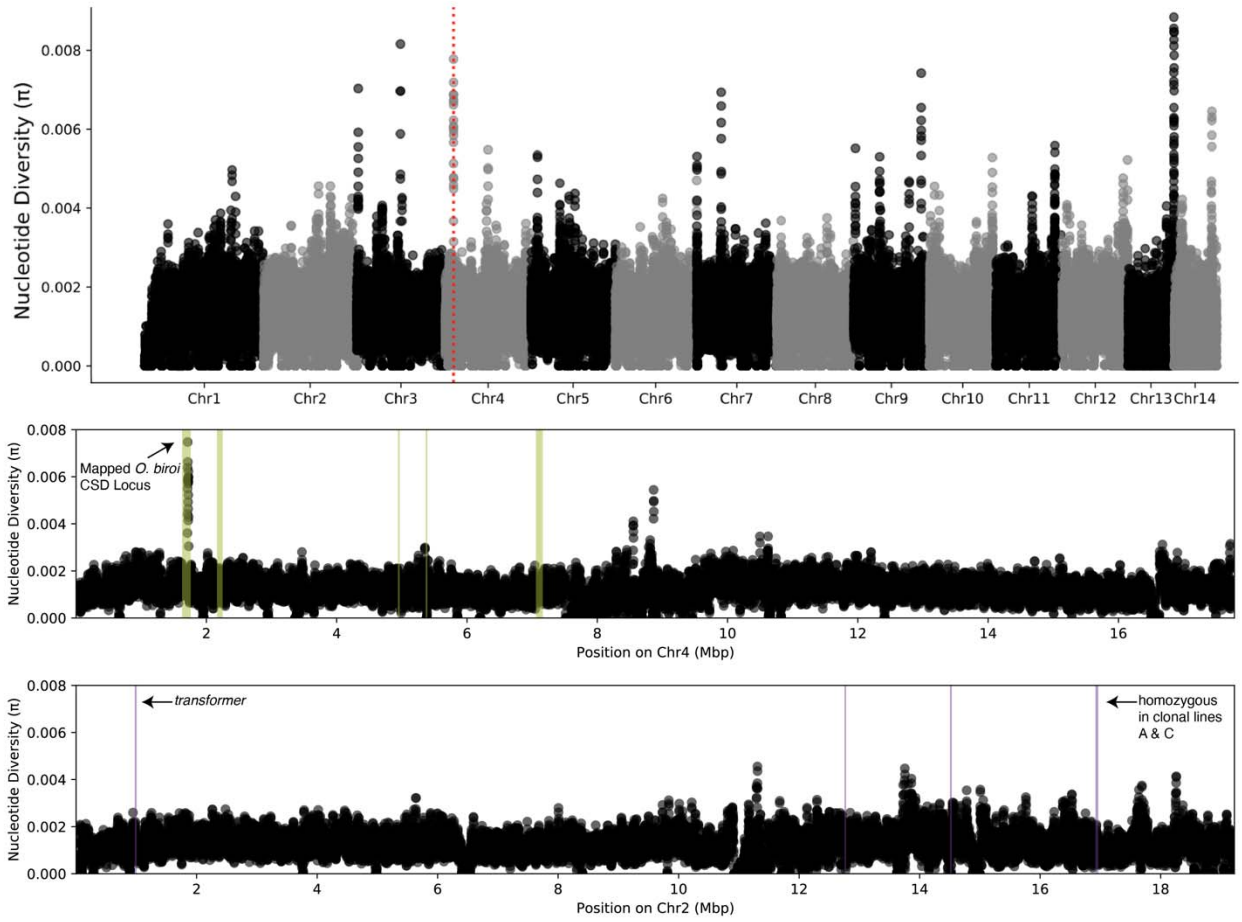

Supplementary Fig. S3. Genome-wide nucleotide diversity. Nucleotide diversity across the genome in 5kb windows with a 1kb sliding interval. In the genome-wide plot (top), the red line depicts the peak of the CSD index from genetic mapping. In the zoomed-in plots for chromosomes 4 (middle) and 2 (bottom), the green and purple vertical shading indicates homology to *V. emeryi* CSD QTL 2 and 1, respectively.

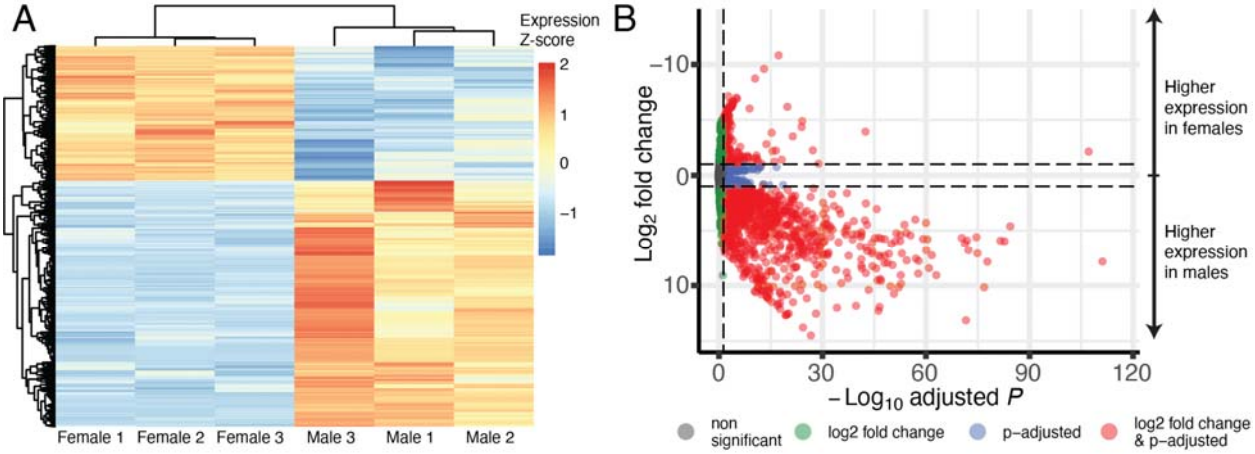

C

Pos. on chromosome 4	Gene Name	Gene ID
Chr4:1607254-1609373	unchar. protein	LOC105285599
Chr4:1609611-1612715	unchar. protein	LOC105285600
Chr4:1619377-1621011	paraneoplastic antigen Ma6E	LOC105285601
Chr4:1621560-1634471	ataxin-7	LOC105285602
Chr4:1637384-1672949	Kank	LOC105285603
Chr4:1673043-1674418	Bet1	LOC105285604
Chr4:1674523-1676002	prob. ribosome prod. factor 1	LOC105285607
Chr4:1675932-1678296	THUMP	LOC105285605
Chr4:1687395-1693282	unchar. lncRNA	LOC105285608
Chr4:1727256-1729679	Creld	LOC113561733
Chr4:1729888-1737844	alphaCOP	LOC105283852
Chr4:1730326-1732211	unchar. protein	LOC105283851
Chr4:1738076-1749057	**Host cell factor**	***LOC105283850***
Chr4:1749634-1750382	**l(2)37Cg**	***LOC105283849***
Chr4:1750527-1752116	ribosomal protein S2	LOC105283847
Chr4:1752262-1755091	guanine deaminase	LOC105283846
Chr4:1755270-1770406	**unchar. protein**	***LOC105283844***

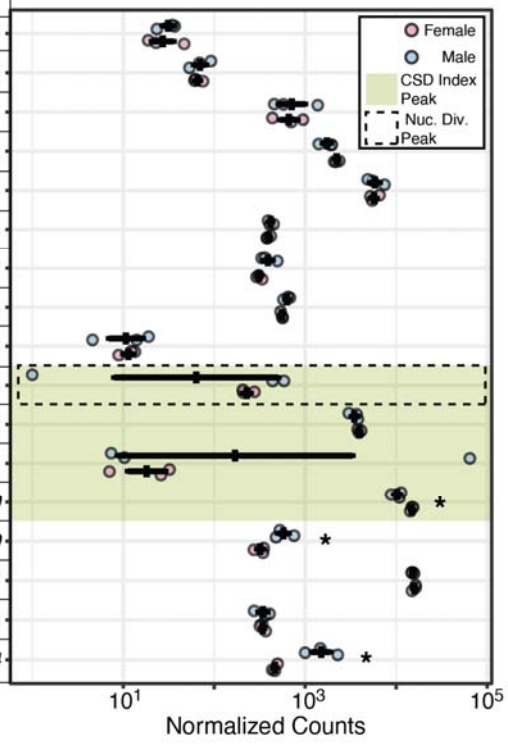

<u>Supplementary Fig. S4.</u> Sex-specific gene expression. (**A**) Heatmap of genes that were significantly differentially expressed between sexes (adjusted p-value < 0.05). Each row represents a gene, and each column represents a sample. The trees at the left and the top of the heat map depict hierarchical clustering of genes and samples, respectively. Z-scores of log-transformed expression levels are shown as a color gradient. (**B**) Volcano plot depicting differential gene expression between males and females. Each gene is represented by a dot,

which is colored gray if not differentially expressed, green if the expression difference is at least 2-fold ($\log_2 \geq 1$), or blue if the expression difference is statistically significant (adjusted p-value < 0.05). Red indicates genes that are significantly differentially expressed and have at least a 2-fold difference in gene expression. (**C**) Expression levels of genes in the vicinity of the CSD index peak. Normalized counts are shown for each male and female sample, with error bars depicting the mean and SEM for each sex. The genomic coordinates, name, and ID are given for each gene. Genes with significantly different expression between sexes (adjusted p-value < 0.05) are bolded in the table and marked with an asterisk on the plot. The CSD index peak is shown in green, and the dashed box denotes the peak of nuclear diversity.

952 **Supplementary Tables**

Primer Name	5.4 Scaffold	5.4 Position	Forward 5'-3'	Reverse 5'-3'	Genotyping Method
Obir Ploidy 12SV	Chr12	12801234	TAGATCGAGT GAGGTATCTT	AGCGTTAA GAGTAGAT TAAG	Visualize differently sized alleles (i.e., different versions of a structural variant [SV]) using gel electrophoresis
Obir Ploidy 4RE	Chr4	5840887	CCACCCTCTC TCTCGTCTC	TGCCGATT CATATTTC GAGATAAA C	Separately digest products with the restriction enzymes (REs) EcoRI and BsmI and visualize genotypes via gel electrophoresis
Obir Ploidy 5RE	Chr5	1963279	GCGATAGAA GAGTGCTCGT ATT	GCCAGTCA GTCTGTCA TTCA	Separately digest products with the restriction enzymes (REs) EcoRI and AvaII and visualize genotypes via gel electrophoresis
Obir Ploidy 2SNP	Chr2	18082503	CACGTACAAT GAGGGAACC TAA	TCGCGATC ATGAAATC TAACCT	Sanger sequence and call SNPs
Obir Ploidy 12SNP	Chr12	8100152	GTCAGTGCGC TGTTCATTTC	AGATTATA GGGCGTTC CAATTCT	Sanger sequence and call SNPs
Obir Ploidy 14SNP	Chr14	6377499	CACGTGAACG CTACGATGAA	GGGTTGAG GATGTCTA AGGTAATG	Sanger sequence and call SNPs
Obir Ploidy 13SNPa	Chr13	6262370	CGTTACACTC CTGTGTCGAA TC	GCACGTAG CATTCTCTC TTTCT	Sanger sequence and call SNPs
Obir Ploidy 13SNPb	Chr13	7173724	GCCATACATC CTGCACTCTT AC	CGACGAGC ATGCGTCT AAA	Sanger sequence and call SNPs

953 **Supplementary Table S1. Primers for ploidy assessment via heterozygosity.** 5.4 refers to the

954 reference genome version (GCA_003672135.1).

Sample name	Library prep method	Clonal line	Stock colony	Sample type	Mean read depth	BioProject
LineA_DiploidFemale_1	Nextera Flex	A	C16	Diploid Female	30.1	PRJNA923657
LineA_DiploidFemale_2	Nextera Flex	A	C16	Diploid Female	27.4	PRJNA923657
LineB_DiploidFemale_1	Nextera Flex	B	STC6	Diploid Female	28.3	PRJNA923657
LineA_DiploidFemale_6	Nextera Flex	A	C18	Diploid Female	30	PRJNA923657
LineA_DiploidFemale_5	Nextera Flex	A	C1	Diploid Female	41.5	PRJNA923657
LineA_DiploidFemale_3	Nextera Flex	A	C16	Diploid Female	26.6	PRJNA947942
LineA_DiploidFemale_4	Nextera Flex	A	C16	Diploid Female	24.1	PRJNA947942
LineB_DiploidFemale_2	Nextera Flex	B	STC6	Diploid Female	27	PRJNA947942
LineB_DiploidFemale_3	Nextera Flex	B	STC6	Diploid Female	47.1	PRJNA947942
LineA_HaploidMale_1	Nextera Flex	A	C16	Haploid Male	26.1	PRJNA947942
LineA_HaploidMale_2	Nextera Flex	A	C16	Haploid Male	26.1	PRJNA947942
LineA_HaploidMale_3	Nextera Flex	A	C16	Haploid Male	27.6	PRJNA947942
LineA_HaploidMale_4	Nextera Flex	A	C16	Haploid Male	25.8	PRJNA947942
LineB_HaploidMale_1	Nextera Flex	B	STC6	Haploid Male	26.3	PRJNA947942
LineB_HaploidMale_2	Nextera Flex	B	STC6	Haploid Male	27.6	PRJNA947942
LineB_HaploidMale_3	Nextera Flex	B	STC6	Haploid Male	31.7	PRJNA947942
LineB_DiploidFemale_5	Nextera Flex	B	STC12	Diploid Female	42.4	PRJNA947942
LineB_DiploidFemale_4	Nextera Flex	B	STC1	Diploid Female	31.7	PRJNA947942
LineA_HaploidMale_5	Nextera Flex	A	C1	Haploid Male	30.3	PRJNA947942
LineA_HaploidMale_6	Nextera Flex	A	C18	Haploid Male	25.3	PRJNA947942
LineB_HaploidMale_4	Nextera Flex	B	STC1	Haploid Male	31	PRJNA947942

LineB_HaploidMale_5	Nextera Flex	B	STC12	Haploid Male	32.8	PRJNA947942
DiploidMale_1	Nextera Flex	A	C16	Diploid Male	57.9	PRJNA1075055
DiploidMale_2	Nextera Flex	A	C16	Diploid Male	32.7	PRJNA1075055
DiploidMale_3	Nextera Flex	A	C16	Diploid Male	31.5	PRJNA1075055
DiploidMale_4	Nextera Flex	A	C18	Diploid Male	38.3	PRJNA1075055
DiploidMale_5	Nextera Flex	A	C17	Diploid Male	47.7	PRJNA1075055
DiploidMale_6	Nextera Flex	A	C16	Diploid Male	28.4	PRJNA1075055
DiploidMale_7	Nextera Flex	A	C16	Diploid Male	32.0	PRJNA1075055
DiploidMale_8	Nextera Flex	A	C2	Diploid Male	30.2	PRJNA1075055
DiploidMale_9	Nextera Flex	A	C16	Diploid Male	41.6	PRJNA1075055
DiploidMale_10	Nextera Flex	A	C16	Diploid Male	28.1	PRJNA1075055
DiploidMale_11	Nextera Flex	A	C18	Diploid Male	40.2	PRJNA1075055
DiploidMale_12	Nextera Flex	A	C16	Diploid Male	38.5	PRJNA1075055
DiploidMale_13	Nextera Flex	A	C16	Diploid Male	35.4	PRJNA1075055
DiploidMale_14	Nextera Flex	A	C16	Diploid Male	34.4	PRJNA1075055
DiploidMale_15	Nextera Flex	A	C1	Diploid Male	31.5	PRJNA1075055
DiploidMale_16	Nextera Flex	A	C1	Diploid Male	32.2	PRJNA1075055
LineC_DiploidFemale	Nextera Flex	C	?	Diploid Female	39.4	PRJNA1075055
LineD_DiploidFemale_2	Nextera Flex	D	BG9	Diploid Female	35.2	PRJNA1075055
LineD_DiploidFemale_1	Nextera Flex	D	?	Diploid Female	36.9	PRJNA1075055
LineI_DiploidFemale	Nextera Flex	I	?	Diploid Female	36.1	PRJNA1075055
LineM_DiploidFemale	Nextera Flex	M	?	Diploid Female	32.3	PRJNA1075055

LineB_HaploidMale	Nextera Flex	B	?	Haploid Male	28.3	PRJNA1075055
LineC_HaploidMale	Nextera Flex	C	C9	Haploid Male	27.6	PRJNA1075055
LineD_HaploidMale_1	Nextera Flex	D	BG7	Haploid Male	25.2	PRJNA1075055
LineD_HaploidMale_2	Nextera Flex	D	BG9	Haploid Male	34.9	PRJNA1075055
LineI_HaploidMale	Nextera Flex	I	BG2	Haploid Male	21.2	PRJNA1075055
LineM_HaploidMale_1	Nextera Flex	M	BG14	Haploid Male	70.7	PRJNA1075055
LineM_HaploidMale_2	Nextera Flex	M	BG14	Haploid Male	34.0	PRJNA1075055
LineB_DiploidFemale	Nextera Flex	B	STC6	Diploid Female	42.8	PRJNA1075055

Supplementary Table S2. Metadata for all DNA whole-genome shotgun sequencing libraries included in this study. Question marks indicate male samples for which the clonal line is known, but the stock colony of origin was not recorded.

V. emeryi **CSD QTL**	***V. emeryi*** **GeneID**	**OrthoFinder** ***O. biroi*** **"Ortholog"**	***O. biroi*** **genomic locus**
2	LOC105559778	LOC105285603	Chr4:1637384-1672949
2	LOC105559779	LOC105285604	Chr4:1673043-1674418
2	LOC105559781	LOC105285607	Chr4:1674523-1676002
2	LOC105559780	LOC105285605	Chr4:1675932-1678296
2	LOC105559782	LOC105283856, LOC113561733	Chr4:1727256-1729679; Chr4:22762-24749
2	LOC105559784	LOC105283852	Chr4:1729888-1737844
2	LOC105559783	LOC105283851	Chr4:1730326-1732211
2	LOC105559785	LOC105283850	Chr4:1738076-1749057
2	LOC105559786	LOC105282554	Chr4:7069030-7075460
2	LOC105559787	LOC105282557	Chr4:7075106-7080018
2	LOC105559788	LOC105286165	Chr4:4951574-4955391
2	LOC105559790	LOC105282568	Chr4:7141680-7152824
2	LOC105559789	LOC105282568	Chr4:7141680-7152824
2	LOC105559791	LOC105283915	Chr4:5377245-5381427
2	LOC105559793	LOC105283797	Chr4:2173362-2237652
1	LOC105558826	LOC105287916	Chr2:985469-993787
1	LOC105558815	LOC105283998	Chr2:14515051-14517463
1	LOC105558816	LOC105283997, LOC113563596	Chr2:14517342-14519998; Chr2:19219509-19221771
1	LOC105558817	LOC105283996, LOC113563597	Chr2:14519947-14522109; Chr2:19217723-19219230
1	LOC105558818	LOC105283999	Chr2:14522233-14522882
1	LOC105558819	LOC105278142	Chr2:16951611-16953740
1	LOC105558820	LOC105278143	Chr2:16947572-16951531
1	LOC105558821	LOC105278141	Chr2:16939029-16945082
1	LOC105558822	LOC105287131	Chr2:12765464-12768244
1	LOC105558823	LOC105278140	Chr2:16929798-16936497

Supplementary Table S3. ***O. biroi*** **orthologs of genes located in the two** ***V. emeryi*** **CSD QTLs.**

	Gene_type	RU	RefSeq	GenBank
Genes	guide_RNA	0	1	0
	lncRNA	1767	1430	0
	miRNA	239	0	0
	misc_RNA	0	44	0
	piRNA	23596	0	0
	protein_coding	12839	11927	13022
	pseudogene	0	373	77
	rRNA	108	109	0
	snoRNA	15	16	0
	snRNA	22	26	0
	tRNA	194	202	0
Total Genes		**38780**	**14128**	**13099**
Transcripts	lncRNA	3795	1751	0
	miRNA	239	0	0
	mRNA	63620	24215	13099
	piRNA	23596	0	0
	rRNA	108	109	0
	snoRNA	15	16	0
	snRNA	22	26	0
	tRNA	194	202	0
	guide_RNA	0	1	0
	transcript	0	818	0
Total transcripts		**91589**	**27135**	**13099**
Total multi-exon transcripts		**65882**	**25945**	**11923**

960 **Supplementary Table S4. Improvements over previous genome annotations, with the new**

961 **(RU) annotation featuring genes and transcripts not found in previous annotation versions.**

Gene Name	Gene ID	Log 2-Fold Change	p-value	p-adjusted
unchar. protein	LOC105285599	0.11	0.84	0.92
unchar. protein	LOC105285600	0.11	0.73	0.85
paraneoplastic antigen Ma6E	LOC105285601	0.21	0.67	0.82
ataxin-7	LOC105285602	-0.33	0.063	0.17
Kank	LOC105285603	0.05	0.82	0.91
Bet1	LOC105285604	0.08	0.54	0.72
prob. ribosome prod. factor	LOC105285607	0.34	0.12	0.27
THUMP	LOC105285605	0.19	0.13	0.28
unchar. lncRNA	LOC105285608	0.12	0.87	0.93
Creld	LOC113561733	0.56	0.77	0.88
alphaCOP	LOC105283852	-0.17	0.21	0.40
unchar. protein	LOC105283851	9.95	NA	NA
Host cell factor	LOC105283850	-0.52	2.1E-04	1.8E-03
l(2)37Cg	LOC105283849	0.86	5.7E-04	4.2E-03
ribosomal protein S2	LOC105283847	-0.06	0.50	0.69
guanine deaminase	LOC105283846	0.03	0.88	0.94
unchar. protein	LOC105283844	1.77	6.1E-08	1.0E-07

Supplementary Table S5. Differential gene expression near the CSD index peak.

The log 2-fold change in expression levels between male and female samples, p-values (Wald test), and adjusted p-values (Benjamini-Hochberg adjustment) for 17 genes in the vicinity of the CSD index peak. The p-values are “NA” for LOC105283850 because one of the samples is an extreme outlier detected by Cook’s distance.

Gene Name	Gene ID	Exon	Log 2-Fold Change	p-value	p-adjusted
unchar. protein	LOC105285599	E001	-0.24	0.37	0.84
		E002	0.09	0.6	0.91
		E003	0.21	0.63	0.92
unchar. protein	LOC105285600	E001	-0.59	0.32	0.82
		E002	-0.23	0.78	0.96
		E003	0.51	0.15	0.72
		E004	0.03	0.87	0.98
		E005	0.06	0.73	0.95
		E006	-0.54	0.31	0.82
		E007	-0.48	0.35	0.83
		E008	0.11	0.91	0.99
		E009	-0.66	0.65	0.92
		E010	0.08	0.92	0.99
		E011	0.11	0.91	0.99
paraneoplastic antigen Ma6E	LOC105285601	E001	-0.28	0.06	0.51
		E002	0.18	0.06	0.5
ataxin-7	LOC105285602	E001	2.03	0.1	0.63
		E002	0.12	0.98	1
		E003	0.06	0.75	0.95
		E004	0.05	0.69	0.94
		E005	-0.04	0.48	0.87
		E006	-0.48	0.01	0.17
		E007	0.12	0.55	0.89
Kank	LOC105285603	E001	-0.93	0.24	0.79
		E002	-0.65	0.05	0.47
		E003	-0.14	0.72	0.94
		E004	-1.04	0.44	0.86
		E005	-1.6	0.29	0.81
		E006	-0.55	0.08	0.57
		E007	-0.67	0.04	0.4
		E008	-0.63	0.08	0.58
		E009	0.01	0.88	0.98
		E010	-0.15	0.34	0.83
		E011	-0.28	0.2	0.76
		E012	-0.27	0.2	0.76
		E013	-0.27	0.18	0.74
		E014	0.07	0.3	0.81

		E015	0.11	0.07	0.54
		E016	0.18	0.26	0.8
		E017	NA	NA	NA
Bet1	LOC105285604	E001	2.7	0.05	0.47
		E002	0	0.99	1
		E003	-0.04	0.67	0.93
		E004	-0.01	0.82	0.97
		E005	0.05	0.94	1
		E006	9.44	0.23	0.78
prob. ribosome prod. factor	LOC105285607	E001	0.24	0.77	0.96
		E002	-0.12	0.77	0.96
		E003	0.05	0.7	0.94
		E004	0	1	1
		E005	0.3	0.55	0.89
THUMP	LOC105285605	E001	1.26	0.04	0.42
		E002	-0.12	0.49	0.87
		E003	-0.09	0.55	0.89
		E004	0.03	0.79	0.96
		E005	0.13	0.19	0.75
		E006	-0.03	0.96	1
		E007	-0.09	0.76	0.95
		E008	-0.09	0.68	0.93
		E009	3.9	0.000257	0.00951
unchar. lncRNA	LOC105285608	E001	-1.46	0.08	0.56
		E002	0.28	0.06	0.5
Creld	LOC113561733	E001	-0.06	0.62	0.92
		E002	-0.01	0.86	0.98
		E003	0.09	0.32	0.82
		E004	-0.15	0.6	0.91
alphaCOP	LOC105283852	E001	-0.29	0.3	0.81
		E002	-0.23	0.33	0.83
		E003	-0.21	0.25	0.79
		E004	-0.15	0.16	0.73
		E005	0.14	0.19	0.75
		E006	0.32	0.3	0.81
		E007	0.74	0.14	0.69
unchar. protein	LOC105283851	E001	-0.07	0.76	0.96
		E002	0.14	0.76	0.96
Host cell factor	LOC105283850	E001	-0.34	0.28	0.8

		E002	-0.33	0.24	0.79
		E003	-0.25	0.38	0.84
		E004	-0.34	0.36	0.84
		E005	-0.19	0.5	0.88
		E006	-0.19	0.39	0.85
		E007	0.75	0.12	0.67
		E008	-0.23	0.33	0.82
		E009	0.3	0.39	0.85
		E010	-0.05	0.93	1
		E011	0.44	0.34	0.83
		E012	0	0.59	0.91
		E013	0	0.35	0.83
		E014	0.45	0.12	0.67
		E015	0.04	0.2	0.77
		E016	-0.35	0.56	0.9
		E017	0.14	0.07	0.55
		E018	0.11	0.48	0.87
		E019	0.35	0.38	0.84
l(2)37Cg	LOC105283849	E001	0.04	0.54	0.89
		E002	-0.03	0.6	0.91
		E003	0	0.94	1
ribosomal protein S2	LOC105283847	E001	0.1	0.54	0.89
		E002	-0.03	0.45	0.86
		E003	-0.06	0.63	0.92
		E004	3.68	0.00233	0.06
guanine deaminase	LOC105283846	E001	0.29	0.31	0.82
		E002	0.15	0.52	0.89
		E003	0.15	0.37	0.84
		E004	0.12	0.55	0.89
		E005	0.1	0.58	0.9
		E006	-0.06	0.62	0.92
		E007	-0.09	0.41	0.85
		E008	-0.17	0.18	0.75
		E009	-0.26	0.07	0.54
unchar. protein	LOC105283844	E001	-0.52	0.000763	0.02
		E002	-0.54	0.00000519	0.000311
		E003	-0.56	0.000378	0.01
		E004	-0.91	0.00693	0.13
		E005	-0.85	0.00588	0.11

		E006	-0.92	0.000107	0.00449
		E007	-0.91	0.00434	0.09
		E008	-0.8	0.00161	0.04
		E009	-0.53	0.00458	0.1
		E010	-0.54	0.0000288	0.00143
		E011	-0.46	0.000237	0.00887
		E012	0.57	7.31E-07	0.0000543
		E013	0.79	0.00000443	0.00027
		E014	1.11	1.32E-07	0.0000115
		E015	1.07	3.96E-07	0.000031
		E016	0.86	0.000705	0.0219
		E017	0.8	0.000814	0.0245
		E018	1.29	0.000153	0.00613
		E019	1.29	0.000454	0.0152
		E020	1.13	0.000177	0.00694
		E021	0.99	0.00261	0.06
		E022	-0.89	0.55	0.89
		E023	1.32	0.000135	0.00547
		E024	1.11	0.07	0.55
		E025	-0.57	0.44	0.86
		E026	-0.24	0.32	0.82
		E027	0.09	0.00973	0.165
		E028	0.21	0.0003	0.0107
		E029	-0.59	2.27E-08	0.00000229
		E030	-0.23	0.00000842	0.000479
		E031	0.51	0.00158	0.0418

<u>Supplementary Table S6.</u> Differential gene expression near the CSD index peak.

The log 2-fold change in expression levels between male and female samples, p-values (likelihood ratio test), and adjusted p-values (Benjamini-Hochberg adjustment) for each exon of 17 genes in the vicinity of the CSD index peak. The p-values are “NA” for one of the exons of LOC105285603 because there is negligible expression of that exon (basemean=0).

Analysis	**Program**	**Version**	**Analysis Available At:**
Genetic Mapping	Trimmomatic	v0.36	https://github.com/kipdlacy/SexDeterminationMapping_Obiroi
Genetic Mapping	bwa	v0.7.12-r1039	https://github.com/kipdlacy/SexDeterminationMapping_Obiroi
Genetic Mapping	GATK	v4.2	https://github.com/kipdlacy/SexDeterminationMapping_Obiroi
Genetic Mapping	vcftools	v0.1.17	https://github.com/kipdlacy/SexDeterminationMapping_Obiroi
Genetic Mapping	pyvcf	v0.6.8	https://github.com/kipdlacy/SexDeterminationMapping_Obiroi
Genetic Mapping	pybedtools	v0.9.0	https://github.com/kipdlacy/SexDeterminationMapping_Obiroi
Genetic Mapping	pandas	v1.1.5	https://github.com/kipdlacy/SexDeterminationMapping_Obiroi
Genetic Mapping	numpy	v.1.19.5	https://github.com/kipdlacy/SexDeterminationMapping_Obiroi
Genetic Mapping	bcftools	v0.1.19-96b5f2294a	https://github.com/kipdlacy/SexDeterminationMapping_Obiroi
Genetic Mapping	samtools	v1.8	https://github.com/kipdlacy/SexDeterminationMapping_Obiroi
Genetic Mapping	OrthoFinder	v2.5.5	https://github.com/kipdlacy/SexDeterminationMapping_Obiroi
Genetic Mapping	scikit-allel	v1.3.5	https://github.com/kipdlacy/SexDeterminationMapping_Obiroi
Genetic Mapping	blast	v2.5.0	https://github.com/kipdlacy/SexDeterminationMapping_Obiroi
Genetic Mapping	mummer	v4.0.0rc1	https://github.com/kipdlacy/SexDeterminationMapping_Obiroi
Genetic Mapping	python	v3.6.15	https://github.com/kipdlacy/SexDeterminationMapping_Obiroi
Genetic Mapping	R	v4.3.2	https://github.com/kipdlacy/SexDeterminationMapping_Obiroi
Genetic Mapping	karyoploteR	1.28.0	https://github.com/kipdlacy/SexDeterminationMapping_Obiroi
Genetic Mapping	ggplot2	v3.5.0	https://github.com/kipdlacy/SexDeterminationMapping_Obiroi
Genetic Mapping	ggbeeswarm	v0.7.2	https://github.com/kipdlacy/SexDeterminationMapping_Obiroi
Genetic Mapping	matplotlib	v3.3.4	https://github.com/kipdlacy/SexDeterminationMapping_Obiroi
Genome Annotation	pbmm2	v1.12.0	https://github.com/RockefellerUniversity/Obiroi_GeneModels_2025
Genome	stringtie2	v2.2.1	https://github.com/RockefellerUniversity/Obiroi_Ge

Annotation			neModels_2025
Genome Annotation	samtools	v1.6	https://github.com/RockefellerUniversity/Obiroi_GeneModels_2025
Genome Annotation	hisat2	v2.2.1	https://github.com/RockefellerUniversity/Obiroi_GeneModels_2025
Genome Annotation	transdecoder	v5.7.1	https://github.com/RockefellerUniversity/Obiroi_GeneModels_2025
Genome Annotation	squanti3	v3.5.1	https://github.com/RockefellerUniversity/Obiroi_GeneModels_2025
Genome Annotation	Repeatmasker	v4.1.7-p1	https://github.com/RockefellerUniversity/Obiroi_GeneModels_2025
Genome Annotation	FEELnc	v0.2.1	https://github.com/RockefellerUniversity/Obiroi_GeneModels_2025
Genome Annotation	BUSCO	v5.4.7	https://github.com/RockefellerUniversity/Obiroi_GeneModels_2025
Genome Annotation	CLIPflexR	v0.1.20	https://github.com/RockefellerUniversity/Obiroi_GeneModels_2025
Genome Annotation	miRDeep2	v0.1.3	https://github.com/RockefellerUniversity/Obiroi_GeneModels_2025
Genome Annotation	Pilfer	v1.0	https://github.com/RockefellerUniversity/Obiroi_GeneModels_2025
Genome Annotation	R	v4.0	https://github.com/RockefellerUniversity/Obiroi_GeneModels_2025
Genome Annotation	Bioconductor	v3.19	https://github.com/RockefellerUniversity/Obiroi_GeneModels_2025
Differential Gene Expression	multiqc	v1.9	https://github.com/jina-leemon/CSD_biroi_male-female-RNA-seq
Differential Gene Expression	RSEM	v1.2.28	https://github.com/jina-leemon/CSD_biroi_male-female-RNA-seq
Differential Gene Expression	STAR	v2.5.0a	https://github.com/jina-leemon/CSD_biroi_male-female-RNA-seq
Differential Gene Expression	R	v4.3.3	https://github.com/jina-leemon/CSD_biroi_male-female-RNA-seq
Differential Gene Expression	GenomicFeatures	v1.52.2	https://github.com/jina-leemon/CSD_biroi_male-female-RNA-seq
Differential Gene Expression	tximport	v1.28.0	https://github.com/jina-leemon/CSD_biroi_male-female-RNA-seq
Differential Gene Expression	DESeq2	v1.40.2	https://github.com/jina-leemon/CSD_biroi_male-female-RNA-seq

Differential Gene Expression	EnhancedVolcano	v1.18.0	https://github.com/jina-leemon/CSD_biroi_male-female-RNA-seq
Differential Gene Expression	pheatmap	v1.0.12	https://github.com/jina-leemon/CSD_biroi_male-female-RNA-seq
Differential Gene Expression	dplyr	v1.1.4	https://github.com/jina-leemon/CSD_biroi_male-female-RNA-seq
Differential Gene Expression	reshape2	v1.4.4	https://github.com/jina-leemon/CSD_biroi_male-female-RNA-seq
Differential Gene Expression	tidyr	v1.3.1	https://github.com/jina-leemon/CSD_biroi_male-female-RNA-seq
Differential Gene Expression	tibble	v3.2.1	https://github.com/jina-leemon/CSD_biroi_male-female-RNA-seq
Differential Gene Expression	ggbreak	v.0.1.2	https://github.com/jina-leemon/CSD_biroi_male-female-RNA-seq
Differential Exon Usage	HTSeq	v2.0.5	https://github.com/jina-leemon/CSD_biroi_male-female-RNA-seq
Differential Exon Usage	DEXSeq	v.1.46.0	https://github.com/jina-leemon/CSD_biroi_male-female-RNA-seq
Differential Exon Usage	stageR	v.1.22.0	https://github.com/jina-leemon/CSD_biroi_male-female-RNA-seq

973 **Supplementary Table S7. Versions of software used for genomics analyses.**

974